International Journal of
Molecular Sciences

MDPI

Article

Transcriptomic Changes Predict Metabolic Alterations in LC3 Associated Phagocytosis in Aged Mice

Anuradha Dhingra [1], John W. Tobias [2], Nancy J. Philp [3] and Kathleen Boesze-Battaglia [1,*]

[1] Department of Basic and Translational Sciences, University of Pennsylvania, Philadelphia, PA 19104, USA
[2] Penn Genomics and Sequencing Core, Department of Genetics, University of Pennsylvania, Philadelphia, PA 19104, USA
[3] Department of Pathology, Anatomy, and Cell Biology, Thomas Jefferson University, Philadelphia, PA 19107, USA
* Correspondence: battagli@upenn.edu; Tel.: +1-215-898-9167

Abstract: LC3b (*Map1lc3b*) plays an essential role in canonical autophagy and is one of several components of the autophagy machinery that mediates non-canonical autophagic functions. Phagosomes are often associated with lipidated LC3b to promote phagosome maturation in a process called LC3-associated phagocytosis (LAP). Specialized phagocytes, such as mammary epithelial cells, retinal pigment epithelial (RPE) cells, and sertoli cells, utilize LAP for optimal degradation of phagocytosed material, including debris. In the visual system, LAP is critical to maintain retinal function, lipid homeostasis, and neuroprotection. In a mouse model of retinal lipid steatosis-mice lacking LC3b ($LC3b^{-/-}$), we observed increased lipid deposition, metabolic dysregulation, and enhanced inflammation. Herein, we present a non-biased approach to determine if loss of LAP mediated processes modulate the expression of various genes related to metabolic homeostasis, lipid handling, and inflammation. A comparison of the RPE transcriptome of WT and $LC3b^{-/-}$ mice revealed 1533 DEGs, with ~73% upregulated and 27% downregulated. Enriched gene ontology (GO) terms included inflammatory response (upregulated DEGs), fatty acid metabolism, and vascular transport (downregulated DEGs). Gene set enrichment analysis (GSEA) identified 34 pathways; 28 were upregulated (dominated by inflammation/related pathways) and 6 were downregulated (dominated by metabolic pathways). Analysis of additional gene families identified significant differences for genes in the solute carrier family, RPE signature genes, and genes with a potential role in age-related macular degeneration. These data indicate that loss of LC3b induces robust changes in the RPE transcriptome contributing to lipid dysregulation and metabolic imbalance, RPE atrophy, inflammation, and disease pathophysiology.

Keywords: cholesterol trafficking; cholesterol metabolism; peroxisomes; transcriptomics; monocarboxylate transporters; LC3-associated phagocytosis (LAP); inflammation; retinal pigment epithelium (RPE); fatty acid metabolism

Citation: Dhingra, A.; Tobias, J.W.; Philp, N.J.; Boesze-Battaglia, K. Transcriptomic Changes Predict Metabolic Alterations in LC3 Associated Phagocytosis in Aged Mice. *Int. J. Mol. Sci.* **2023**, *24*, 6716. https://doi.org/10.3390/ijms24076716

Academic Editor: Juan J. Salazar

Received: 24 February 2023
Revised: 28 March 2023
Accepted: 28 March 2023
Published: 4 April 2023

1. Introduction

Autophagy, the activity of "self-eating", is vital for cell homeostasis; this catabolic process degrades old, damaged, or abnormal organelles and other substances in the cell cytoplasm [1]. Macroautophagy (hereafter referred to as autophagy or canonical autophagy (CA)) is evolutionarily conserved across eukaryotes and involves formation of a double membrane autophagosome, a specialized structure that engulfs cellular components such as protein aggregates, lipids, and damaged organelles [2]. Upstream signals, such as nutrient deprivation or stress, trigger the activation of a multistep autophagy cascade involving several autophagy related proteins (ATGs), culminating in the lipidation of microtubule-associated protein light chain 3 (LC3/ATG8) to phosphatidylethanolamine (PE) during autophagosome biogenesis, a step necessary to target autophagosomes for

lysosomal degradation [3–6]. Lipid homeostasis requires specialized autophagy processes to maintain mitochondrial and peroxisome health through mitophagy and pexophagy, respectively [5,7].

A sub-set of the autophagy related proteins are involved in a hybrid autophagy-phagocytosis pathway, termed LC3-associated phagocytosis (LAP), considered a non-cannonical autophagy pathway [8–12]. Professional phagocytes such as macrophages, monocytes, and dendritic cells, as well as non-professional/specialized phagocytes, such as mammary epithelial cells, retinal pigment epithelial (RPE) cells, and sertoli cells utilize LAP for optimal degradation of phagocytosed material, including dead cells/cellular debris, and to recycle nutrients, such as vitamin A derivatives [6,11,13–15]. While LAP shares molecular machinery with CA, it is a distinct process; unlike CA, LAP is AMPK–mTORC1–ULK1 independent and unresponsive to nutrient status [8,11,16]. In LAP, a sub-set of autophagy machinery proteins conjugate lipidated LC3 (LC3II) to single membrane phagosome to form a LAPosome followed by degradation in the lysosome [8]. LAP and CA are regulated by RUBCN (Run domain Beclin-1 interacting and cysteine-rich containing protein); this protein promotes LAP and concomitantly suppresses CA [17,18]. Defects in macrophage LAP lead to enhanced pro-inflammatory cytokine production in chronic obstructive pulmonary disease (COPD) and in response to cigarette smoke [10,19]. In vitro knockdown of *LC3b* in lung epithelia sensitized these cells to bleomycin-induced apoptosis [20]. Similarly, the $LC3b^{-/-}$ mouse shows increased susceptibility to lung injury and fibrosis [20]. LAP mediates an anti-inflammatory and immune-suppressive response that, in the context of the tumor microenvironment, leads to evasion of immune surveillance resulting in tumor progression; LAP deficiency results in hyper-inflammation [21–23]. Numerous bacteria have evolved strategies to actively evade (or exploit) host cell LAP as a survival mechanism [9,24].

In the eye, LAP supports visual function and lipid homeostasis in the post-mitotic RPE cells. The RPE, residing in close apposition to photoreceptors, supplies nutrients to the retina, regulates fluid/ion balance, supports the visual cycle, and maintains the blood retinal barrier [11,25,26]. These functions rely on daily phagocytic clearance of lipid-rich photoreceptor outer segment tips over the lifetime of the retina [27]. RPE-LAP requires melanoregulin (Mreg, an LC3 interacting protein)-dependent recruitment of LC3II for subsequent phagosome maturation and phagolysosome formation, leading to degradation of the phagocytosed cargo [12,28]. Some of the degradation by-products are removed from the cell by transport to the choroid, and others are recycled; they replenish essential components and metabolites needed by the neural retina [6,11,29]. Mouse models of defective RPE-LAP (*Atg5ΔRPE*, $Mreg^{-/-}$ and $LC3b^{-/-}$) exhibit increased phagosome accumulation, inadequate recovery of retinoids, and reduced visual capacity [11,12,28,30].

RPE is intimately associated with the neural retina, and RPE-LAP plays an important role in lipid regulation in the eye. Indeed, several studies have demonstrated that lipid dysregulation contributes to the pathogenesis of age-related macular degeneration (AMD) [31–34]. The RPE exploits LAP to efficiently degrade lipid and protein rich OS material daily; it metabolizes OS lipids to generate β-hydroxybutyrate (by ketogenesis), which may support the energy needs of the outer retina [35,36]. The abrogation of LAP, defective processing of lipid rich phagosomes in $LC3b^{-/-}$ RPE, causes phagosome accumulation, resulting in a decrease in fatty acid oxidation and ketogenesis, as well as disrupted lipid homeostasis. This results in an increase in RPE and sub-RPE lipid deposits, elevated levels of lipid peroxidation products, pro-inflammatory sterol, 7-ketocholesterol (7KCh), and decreased levels of lipid pro-survival factors Neuroprotectin D1 (NPD1) and Maresin-1 [28]. Moreover, these mice show a sub-retinal recruitment of microglia [28]. These studies point to a vital role for LAP in lipid regulation with a loss of lipid/cholesterol homeostasis, contributing to an AMD-like phenotype [11,12,28,30]. Over time in aging $LC3b^{-/-}$ mice, a chronic low-grade inflammatory response (para-inflammation) is manifested, which, combined with observed lipid steatosis, is reminiscent of non-alcoholic fatty liver disease [37].

Herein, we investigate how a loss of LC3b affects gene expression using an unbiased, RNAseq based comparative transcriptomics approach, thus allowing us to further uncover the mechanistic aspects of defective LAP leading to inflammation and lipid metabolic dysregulation. We provide a detailed report of the differentially expressed genes (DEGs) and perform gene ontology-based enrichment analyses and hallmark pathway analyses to decipher affected pathways. Our results show that in the *LC3b*$^{-/-}$ mice, inflammatory response, cholesterol homeostasis, and complement activation are upregulated while fatty acid metabolism and oxidative phosphorylation are downregulated. Moreover, the data provides novel insights into gene expression changes in the solute carrier family and some RPE signature genes suggesting metabolic changes resulting from defective LAP. Finally, we identify 8 DEGs that have corresponding risk alleles reported for AMD in a large genome-wide association study (GWAS) [38] and experimentally validate the correlation between gene transcription (based on RNAseq) and protein expression for one of these DEGs. These results point to molecular links between defective LAP and AMD-like pathology and potentially can be extended to other age-related pathologies.

2. Results

2.1. RNAseq Data Source and Quality (High Throughput RNA Sequencing Data Set Preparation for Analysis)

Aged *LC3b*$^{-/-}$ mice show retinal lipid imbalance and enhanced pro-inflammatory micro-environment. This is due to RPE and sub-RPE lipid deposits and a concomitant decrease in the synthesis of protective lipid species, NPD1, and maresin-1 [28]. To identify RPE-specific changes in the *LC3b*$^{-/-}$ mouse at the gene expression level, we prepared RNA from RPE isolated from mouse retina. The experimental design used for RPE cell isolation for subsequent RNA preparation and sequencing is illustrated in Figure 1A. Sequencing was performed using Illumina NovaSeq 6000 SP flow cell with the XP workflow (100 bp single read sequencing) to a minimum depth of 28.54 MR with a median depth of 30.4 MR (+/− 5.8 MR). Total reads for the samples ranged from 26,704,479 to 35,616,153. For each sample, over 85% of reads mapped to the transcriptome. Principal component analysis (PCA) shows the overall variation among the samples with a clear separation in the first two components (Figure 1B).

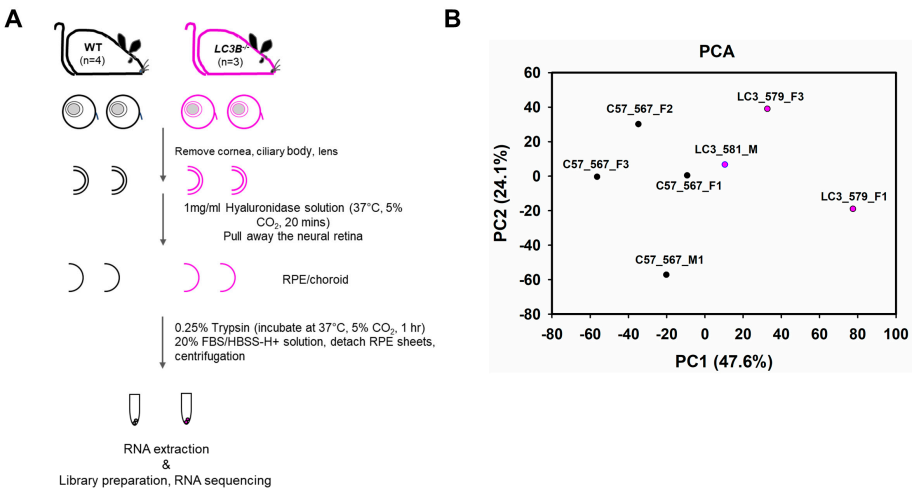

Figure 1. Retinal pigment epithelium (RPE) cell isolation for RNAseq and Principal component analysis. (**A**) Experimental design to isolate RPE from mouse eyes; ~24-month old WT and *LC3b*$^{-/-}$ mice were sacrificed, and the eyeballs were removed and processed to isolate RPE cells by enzymatic treatments as indicated. Total RNA was extracted and used for library preparation and RNA sequencing. (**B**) Principal component analysis (PCA), X-axis, and Y-axis show PC1 and PC2, respectively.

2.2. RNA-Sequencing Analysis to Identify Differentially Expressed Genes (DEGs)

Differential expression between *LC3b*$^{-/-}$ and WT was analyzed using DESeq2. Genes showing fold change of ≤ -1.5 or ≥ 1.5, and an adjusted p-value < 0.05 was considered differentially expressed. There were 1533 DEGs between *LC3b*$^{-/-}$ and WT, 1118 (~73%) upregulated and 415 (27%) downregulated (Figure 2, Volcano plot). A list of DEGs identified in this dataset along with their Log2 fold change and adjusted p-value is provided in Table S1. As expected, *Map1lc3b* was one of the most highly downregulated genes by adjusted p-value; furthermore, there was no compensatory upregulation of a related isoform *Map1lc3a* (gene encoding for LC3a) or other members of the ATG8/LC3 family (*Gabarap*, *Gabarapl1*, *Gabarapl2*) in the *LC3b*$^{-/-}$ mouse (Figure 2) [5,28,39–41].

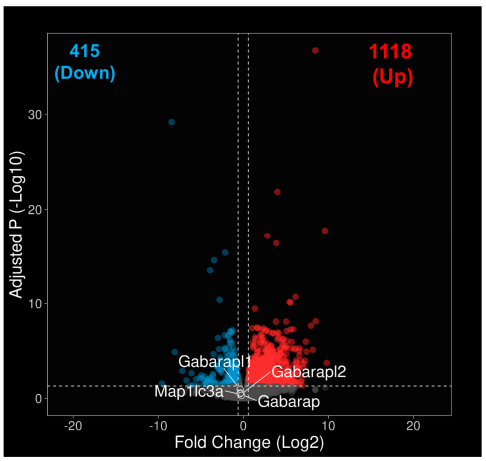

Figure 2. Differentially expressed genes (DEGs) between the *LC3b*$^{-/-}$ and WT RPE. Volcano plot of DEGs between the *LC3b*$^{-/-}$ and WT RPE with –Log10 of the adjusted p value on the Y axis and Log2 of the fold change expression on the X axis. Each point represents a single gene. DEGs were identified by using a cut-off of Padj <0.05 and fold change of ≤ -1.5 or ≥ 1.5 and have been shown in red (upregulated DEGs), cyan (dowregulated DEGs), or grey dots (unchanged genes). Genes that are upregulated in the *LC3b*$^{-/-}$ are on the right (Up) and downregulated genes are on the left (Down). Genes belonging to ATG8/LC3 family (except for *Map1lc3b*) are indicated. *Map1lc3b* with adjusted P (-Log10) of 168.4 is not shown in the volcano plot.

2.3. RNA-Sequencing Reveals Pathways Related to Inflammation and Metabolism

We performed Gene Ontology (GO) based enrichment analysis using the Metascape tool under 3 categories: Molecular Functions (MF), Cellular components (CC), and Biological Processes (BP). Table 1 shows a list of GO terms for top 10 DEGs under each of these categories. Closer examination of these GO terms revealed that the majority overlap with upregulated DEGs. This is not surprising since there are many more upregulated DEGs (>2.5 fold) in our list. Next, we performed a similar enrichment analysis across all upregulated and downregulated genes separately. Figure 3A shows top 5 most enriched GO terms for each of the 3 categories; more than 5 GO terms have been shown in cases where LogP values were exactly the same for more than one term. Interestingly, some of the most enriched GO terms for the upregulated genes are related to inflammation (Inflammatory response and cellular response to cytokine stimulus) and cell–cell adhesion (Figure 3A), whereas the downregulated DEGs were enriched in GO terms related to metabolism, including fatty acid metabolic process, transmembrane transporters, and mitochondria (Figure 3B). There was no significant enrichment of GO terms corresponding to phagosome maturation (GO:0090382) or phagosome lysosome fusion (GO:0090385). Reactome pathway analysis also supported these results; interleukin and cytokine signaling seen in 2 of the top 5 upregulated DEGs (Figure 3C) while metabolism of lipids and fatty acid metabolism was seen in the downregulated DEGs (Figure 3D).

Table 1. Top 10 most enriched Gene ontology terms (GO) (selected based on the *p*-values) across all DEGs. GO terms with up (↑) or down (↓) arrows indicate those enriched with upregulated or downregulated genes, respectively. Analysis was performed using Metascape.

Category	GO	Description	LogP	Enrichment	Z-Score
GO Molecular Functions	GO:0050839	cell adhesion molecule binding (↑)	−22	3.2	12
	GO:0045296	cadherin binding (↑)	−17	3.6	11
	GO:0019900	kinase binding (↑)	−14	2.4	8.9
	GO:0005509	calcium ion binding (↑)	−13	2.4	8.7
	GO:0019901	protein kinase binding (↑)	−12	2.4	8.2
	GO:0004672	protein kinase activity (↑)	−11	2.5	8
	GO:0016773	phosphotransferase activity, alcohol group as acceptor (↑)	−11	2.3	7.7
	GO:0005543	phospholipid binding (↑)	−9.9	2.5	7.5
	GO:0016301	kinase activity (↑)	−9.8	2.2	7.3
	GO:0004175	endopeptidase activity (↑)	−8.9	2.5	7.1
GO Cellular Components	GO:0005911	cell-cell junction (↑)	−22	3.4	12
	GO:0009925	basal plasma membrane (↑) (↓)	−18	4.2	12
	GO:0045178	basal part of cell (↑) (↓)	−17	3.9	11
	GO:0045177	apical part of cell (↑) (↓)	−16	3.2	10
	GO:0016324	apical plasma membrane (↑) (↓)	−16	3.4	10
	GO:0016323	basolateral plasma membrane (↑) (↓)	−15	4	10
	GO:0030055	cell-substrate junction	−14	3	9.2
	GO:0005925	focal adhesion	−14	3	9.2
	GO:0005764	Lysosome (↑) (↓)	−13	2.3	8.4
	GO:0000323	lytic vacuole (↑) (↓)	−13	2.3	8.4
GO Biological Processes	GO:0030855	epithelial cell differentiation (↑)	−18	2.9	11
	GO:0006954	inflammatory response (↑)	−17	3	11
	GO:0071345	cellular response to cytokine stimulus (↑)	−17	2.6	10
	GO:0098609	cell-cell adhesion (↑)	−17	2.9	10
	GO:0009611	response to wounding (↑)	−16	3.1	10
	GO:0001775	cell activation (↑)	−16	2.6	9.7
	GO:0008544	epidermis development (↑)	−16	3.6	10
	GO:0048729	tissue morphogenesis	−16	2.8	9.8
	GO:0008610	lipid biosynthetic process (↓)	−15	2.7	9.6
	GO:0030162	regulation of proteolysis (↑)	−15	2.5	9.2

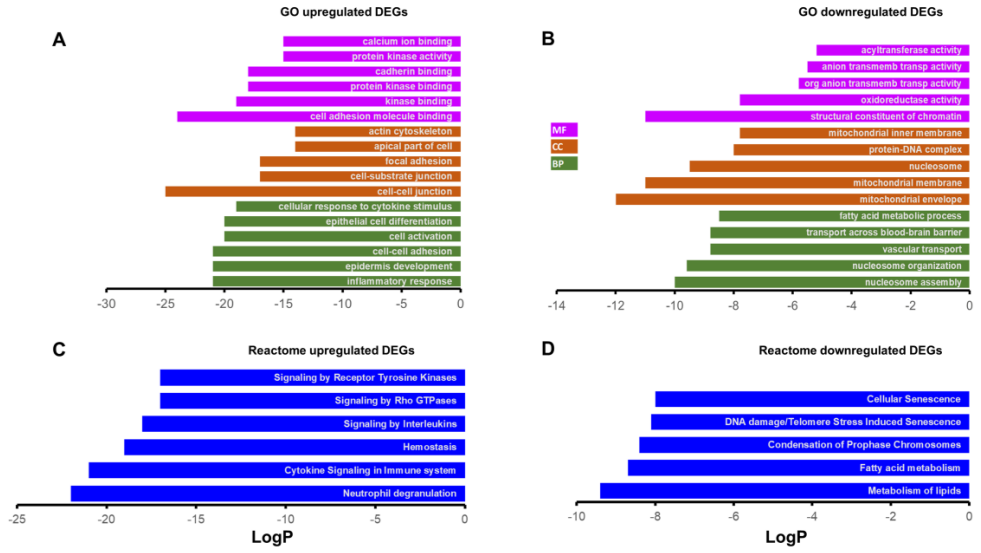

Figure 3. Gene Ontology (GO) and reactome based gene enrichments. The top 5 most enriched GO terms of upregulated DEGs (**A**) and downregulated DEGs (**B**). The top 5 most enriched reactome gene terms for upregulated DEGs (**C**) and downregulated DEGs (**D**). The terms were selected based on the lowest LogP values (>5 GO terms shown in cases where LogP values were exactly same for more than one term). Analysis was performed using Metascape. MF: molecular function; CC: cellular component; BP: biological process.

In addition, an unfiltered list of genes ranked by their DESeq2 statistic was analyzed with GSEA against the hallmark gene collections in the Molecular Signatures Database (MSigDB). GSEA identified 34 significantly different (FDR q-val < 0.05) hallmark pathways; 28 were upregulated (Figure 4, top), and 6 were downregulated (Figure 4, bottom). Upregulated pathways were dominated by inflammation/related pathways (eg, inflammatory response, complement, cholesterol homeostasis); those enriched by down-regulated genes were dominated by metabolic pathways (eg., oxidative phosphorylation, fatty acid metabolism, and peroxisome). We have previously established that LC3b plays a critical role in lipid-mediated homeostasis in the RPE; loss of LC3b leads to decrease in fatty acid oxidation, peroxisomal turn-over defects, age-dependent lipid accumulation, oxidative stress, and pro-inflammatory microenvironment [28,42].

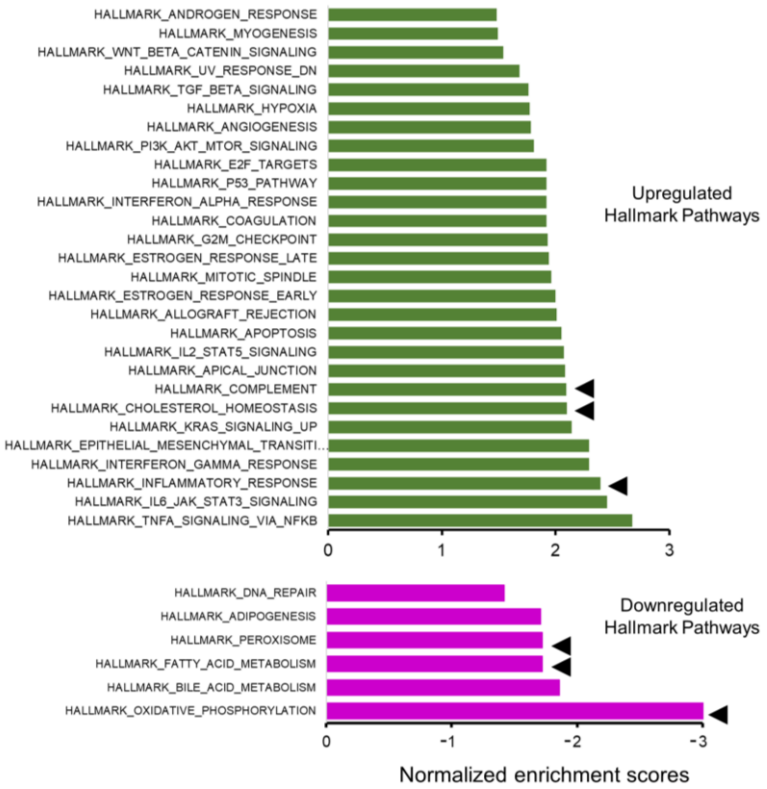

Figure 4. Gene set Enrichment Analysis (GSEA). Bar chart showing absolute normalized enrichment scores for the hallmark pathways that were significantly different between the *LC3b*$^{-/-}$ and WT (false discovery rate or FDR < 0.05); GSEA identified 34 significantly different hallmark pathways: 28 were upregulated (top panel) and 6 were downregulated (bottom panel). Pathways indicated by arrowhead (◂) were selected for further analysis.

LC3b$^{-/-}$-RPE exhibits decrease in fatty acid oxidation and ketogenesis along with chronic low-grade inflammation [28]. To understand the contribution of gene expression changes associated with lipid metabolic imbalance and pro-inflammatory environment, we further examined some of the key hallmark pathways in relation to RPE physiology and metabolism (Figure 4, pathways marked by arrowheads). The hallmark inflammatory response gene set is composed of 196 genes; 112 genes were part of the leading edge with a normalized enrichment score (NES) of 2.39 (Figures 5A and S1A). The hallmark complement gene set includes 187 genes; 85 genes were part of the leading edge with an NES of 2.1 (Figures 5B and S1B). The hallmark cholesterol homeostasis gene set includes 74 genes; 38 genes were part of the leading edge with an NES of 2.1 (Figures 5C and S1C).

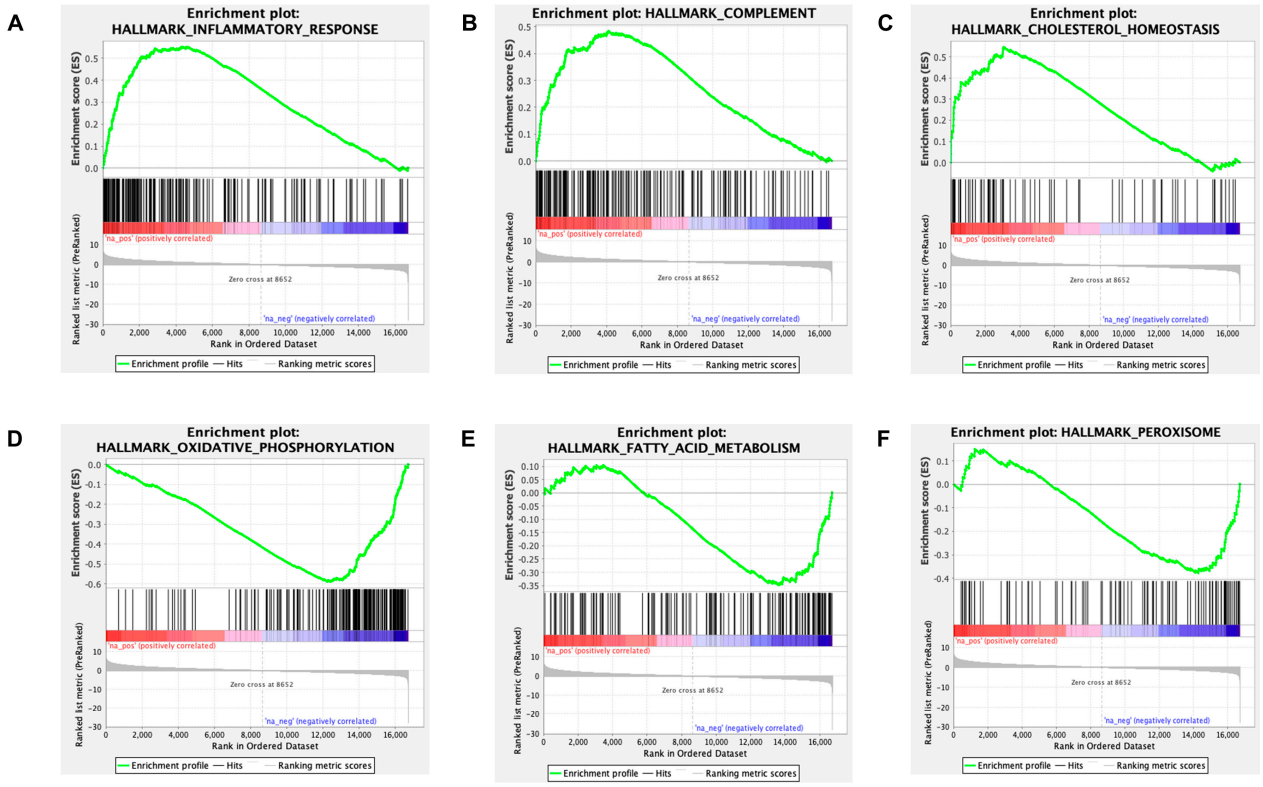

Figure 5. GSEA enrichment profile of upregulated and downregulated pathways. (**A**) A GSEA enrichment plot of the hallmark inflammatory response pathway with a normalized enrichment score 2.39 and an enrichment score of 0.55 indicating a positive relation. The leading edge includes 112 genes. (**B**) A GSEA enrichment plot of the hallmark complement pathway with a normalized enrichment score 2.1 and an enrichment score of 0.48 indicating a positive relation. The leading edge comprised 85 genes. (**C**) A GSEA enrichment plot of the hallmark cholesterol homeostasis pathway with a normalized enrichment score 2.1 and an enrichment score of 0.55 indicating a positive relation. The leading edge comprised 38 genes. (**D**) A GSEA enrichment plot of the hallmark oxidative phosphorylation pathway with a normalized enrichment score −3.02 and an enrichment score of −0.59 indicating a negative relation. The leading edge comprised 138 genes. (**E**) A GSEA enrichment plot of the hallmark fatty acid metabolism pathway with a normalized enrichment score −1.72 and an enrichment score of −0.35, indicating a negative relation. The leading edge comprised 57 genes. (**F**) A GSEA enrichment plot of the hallmark peroxisome pathway with a normalized enrichment score −1.72 and an enrichment score of −0.38 indicating a negative relationship. The leading edge comprised 35 genes.

The hallmark oxidative phosphorylation gene set is composed of 199 genes; 138 genes were part of the leading edge with an NES of −3.02 (Figures 5D and S2A). The hallmark fatty acid metabolism gene set includes 155 genes; 57 genes were part of the leading edge with an NES of −1.72 (Figures 5E and S2B). The hallmark peroxisome gene set is composed of 102 genes; 35 genes were part of the leading edge with an NES of −1.72 (Figures 5F and S2C).

2.4. Several Solute Carrier Family Genes Are Differentially Expressed

Transporters play one of the most essential roles in metabolic homeostasis [43]. Anion transmembrane transporter activity was identified as one of the top GO terms in the pathway enrichment analysis of downregulated DEGs (Figure 3B). As RPE is intimately connected with choroid (basal) and neural retina (apical) and has an important regulatory role in movement of metabolites and ions into and out of retina, we broadened our analysis to look specifically at solute carrier family gene expression. There were 43 DEGs (depicted in the heat map, Figure 6A top) between *LC3b*$^{-/-}$ and WT out of a total of 390 solute carrier

genes ($\chi 2 = 9.599$; two-tailed p value < 0.05). Interestingly, *Slc16a1* and *Slc16a8* encoding for MCT1 and MCT3, respectively, two of the key lactate transporter genes expressed in the RPE [44] are downregulated while *Slc16a11* (encoding for MCT11, an orphan transporter), expression is upregulated in *LC3b*$^{-/-}$ RPE [45]. Moreover, expression of *Bsg*, encoding for Basigin (CD147), a protein required for proper trafficking of MCT1 and MCT3 to the plasma membrane, was also downregulated (Table S1, Figure 6A, bottom) [46,47]. Consistent with the transcriptomic analysis, we observed ~40% decrease in MCT3 protein levels in the *LC3b*$^{-/-}$ compared to the WT control (Figure 6B). Mouse RPE/choroid flat mounts also showed a decrease in MCT3 with a mis-localization of much of the remaining MCT3 as intracellular and not plasma membrane-associated, consistent with the decrease in *Bsg* (Figure 6C).

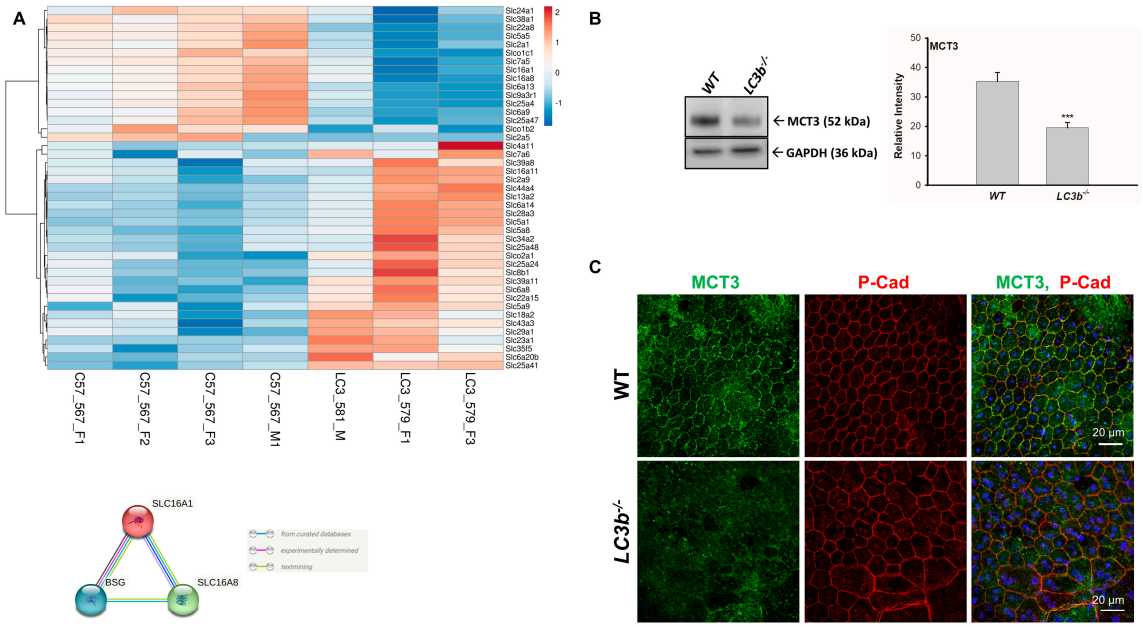

Figure 6. Analysis of the solute carrier family genes. (**A**) Top: Heat map of various solute carrier family DEGs. The variance stabilized counts were converted to heat map colors using Clustvis software. Rows are centered; unit variance scaling is applied to rows. Rows are clustered using correlation distance and average linkage. The intensity scale ranges from low expression (dark blue) to high expression (red) relative to the median of the gene's expression across all samples. Gene names (left) and mouse ID (bottom) are indicated. $\chi 2 = 9.599$ with 1 degrees of freedom, two-tailed p-value = 0.0019. Bottom: String diagram showing nexus between Slc16a1, Slc16a8, and Basigin (Bsg). (**B**) Left: Western blots of RPE/choroid from WT and *LC3b*$^{-/-}$. Immunoblot analysis was performed with antibodies against MCT3 and loading control (GAPDH). Right: Quantification of mean intensity ±SEM of MCT3 relative to GAPDH (N = 3 eyes) *** $p < 0.005$. (**C**) Representative confocal images of RPE/choroid flat mount from WT (top) and *LC3b*$^{-/-}$ (bottom) immuno-stained for MCT3 (green) and P-cadherin (red). Images are projections from 5 µm stacks captured using 60× water objective (NA1.2) on Nikon A1R laser scanning confocal microscope.

2.5. Loss of LC3b Is Associated with Differential Expression of Select RPE Signature and Lipid Metabolism Related Genes

Gene expression alterations in some of the key lactate transporter genes (such as *Slc16a1*) prompted us to evaluate expression of RPE signature and lipid metabolism related genes. We used mouse orthologs from a list of RPE signature genes (human) reported previously [48]. Our analysis revealed significantly different expression profile between *LC3b*$^{-/-}$ and WT ($\chi 2 = 6.43$; two-tailed p value < 0.05) with 19 DEGs among 149 genes in the list. Expression profile of the DEGs is depicted in the heat map (Figure 7A). Gene expression of *Rbp1* (retinoid binding protein 1), *Enpp2* (Ectonucleotide Pyrophosphatase/Phosphodiesterase 2), and *Ptgds* (Prostaglandin D2 Synthase), further suggest

some functional decline in the *LC3b*$^{-/-}$ RPE. Moreover, expression of *Slc6a20b* (Sit1, a proline and betaine transporter) is upregulated (Figure 7A). Interestingly, expression of *Best1* and *Rpe65*, two well studied RPE markers did not change significantly (Figure S3A,B) [49].

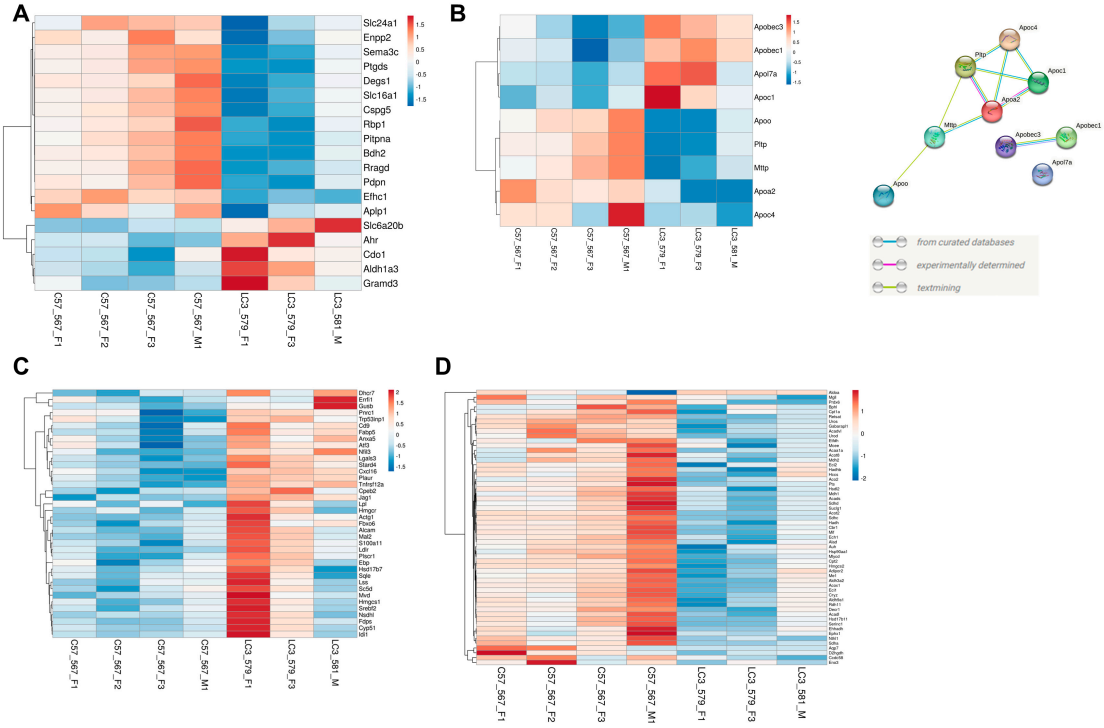

Figure 7. Heat maps depicting DEGs or leading-edge genes in different gene sets. (**A**) Heat map of the DEGs between the *LC3b*$^{-/-}$ and WT from RPE signature gene set. An amount of 19 DEGs out of 149 RPE signature genes were examined; $\chi 2 = 6.43$ with 1 degrees of freedom (two-tailed *p*-value = 0.0112). (**B**) Heat map of the DEGs (between the *LC3b*$^{-/-}$ and WT RPE) overlapping with lipoprotein metabolism associated genes. An amount of 9 DEGs out of 41 lipoprotein metabolism associated genes were examined; $\chi 2 = 13.93$ with 1 degrees of freedom (two-tailed *p*-value = 0.0002). (**C**) Genes in the leading edge of cholesterol homeostasis hallmark pathway (upregulated). (**D**) Genes in the leading edge of fatty acid metabolism hallmark pathway (downregulated). For all the heatmaps, the variance stabilized counts were converted to colors using Clustvis software. Rows are centered; unit variance scaling is applied to rows. Rows are clustered using correlation distance and average linkage. The intensity scale ranges from low expression (dark blue) to high expression (red) relative to the median of the gene's expression across all samples. Gene names (left) and mouse ID (bottom) are indicated.

On a molecular scale, our GSEA analysis showed transcriptional changes in fatty acid metabolism and cholesterol homeostasis. We sought to further explore if LAP-mediated processes modulate the level of genes related to lipid transport/handling. Gene expression profiles for lipoprotein metabolism associated genes, including apolipoproteins (30 genes), apolipoprotein B mRNA editing enzyme catalytic polypeptides 1–4 (4 genes), *Apobr*, *Mttp*, *Pltp* and *Lcat*, *Acat1*, *Acat2*, and *Lrp8* also showed significant differences between *LC3b*$^{-/-}$ and WT with 9 DEGs out of 41 genes examined ($\chi 2 = 13.93$; two-tailed *p* value < 0.05) (Figure 7B, left). PPI string diagram (Figure 7B, right) depicting interaction between the differentially expressed genes *Apoc4*, *Apoc1*, *Apoa2*, *Pltp*, and *Mttp* suggests altered lipoprotein metabolism in the *LC3b*$^{-/-}$ RPE with *Apoa2* potentially playing a central role.

Lipoprotein metabolism is intimately linked to cholesterol biosynthesis and transport. GSEA of cholesterol homeostasis pathways show upregulation of genes for cholesterol biosynthesis (*Hmgcr*, *Hmgcs1*, *Fdps*, *Sqle*, *Cyp51a1*, *Idl1*, *Nsdhl*, and others), as well as genes associated with cholesterol trafficking/import (*Stard4*, *Ldlr*) [50]. Core enrichment subset in the cholesterol homeostasis pathway also includes genes coding for proteins involved

in lipid metabolic disorders, some of which link lipoprotein metabolism with cholesterol homeostasis (*Lpl*, *Ldlr*) and the cholesterol biosynthetic enzymes (*Dhcr7*, *Nsdhl*, and *Ebp*) (depicted as heat map in Figure 7C) [51,52]. GSEA of fatty acid metabolism pathway shows downregulation of genes involved in ketogenesis (*Hmgcs2*), several genes critical for the TCA cycle (*Sdhc*, *Sdha*, *Sdhd*, *Aco2*, *Suclg1*), peroxisomal fatty acid oxidation (*Acox1*, *Acaa1*), and mitochondrial β-oxidation (*Acadl*, *Acadvl*, *Cpt2*, *Cpt1a*) (depicted as heat map in Figure 7D). Acox1 catalyzes desaturation of acyl-CoA esters, which is the initial committed step in peroxisomal fatty acid oxidation [53,54].

2.6. DEGs with Potential Role in Age-Related Retinal Diseases

Dysregulation in lipid/cholesterol homeostasis is linked to age-related diseases and loss of RPE function [55–57]. Several features observed in the *LC3b*$^{-/-}$ RPE, such as reduced phagocytosis, lipid deposits, recruitment of immune cells, and complement pathway activation are reminiscent of AMD-like pathophysiology [28,58–60]. To gain insight into the molecular changes underlying this pathology, we analyzed expression of genes with potential role in AMD.

We started with a list of 41 genes based on a list identified as genes with top priority and statistical significance combined in a genome-wide association study (GWAS) published by the International AMD Genomics Consortium (IAMDGC). Currently, this is both the most recent and largest AMD GWAS study and reported 52 independent genetic signals distributed over 34 loci associated with AMD at genome-wide significance [38,61]. There was a significantly different expression profile between *LC3b*$^{-/-}$ and WT ($\chi 2 = 12.02$; two-tailed p value = 0.0005) with 8 DEGs out of 37 mouse orthologs identified (depicted in the heat map, Figure 8), including *Rdh5*, *Slc16a8*, and *Htra1*. Slc16a8 (MCT3) plays an important role in regulating ionic composition of outer retina and *Slc16a8*$^{-/-}$ mice showed reduced visual function [62]. A subset of patients with *RDH5* (retinol dehydrogenase 5) mutation develop macular atrophy; reduced RDH5 activity is considered a risk factor for AMD [63,64]. Increased protein expression of *HTRA1* (High Temperature Requirement A Serine Peptidase 1), a serine protease, was seen in iPSC-derived RPE cell line from subjects carrying AMD risk-associated 10q26 locus [65].

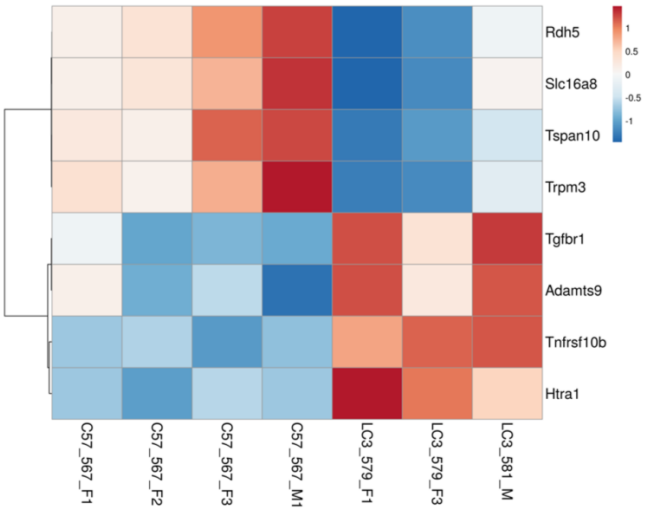

Figure 8. Heat map of the DEGs overlapping with AMD loci genes. AMD loci genes with top priority based on biological and statistical evidence combined (from Fritsche et. al. 2016) were used for the analysis. The variance stabilized counts were converted to heat map colors using Clustvis software. Rows are centered; unit variance scaling is applied to rows. Rows are clustered using correlation distance and average linkage. The intensity scale ranges from low expression (dark blue) to high expression (red) relative to the median of the gene's expression across all samples. Gene names (left) and mouse ID (bottom) are indicated. $\chi 2$ equals 12.02 with 1 degrees of freedom; two-tailed p value = 0.0005.

3. Discussion

Post-mitotic cells such as neurons, RPE cells, and cardiac myocytes utilize autophagic processes to sustain homeostasis; these cells get rid of unwanted material (waste) and recycle cellular components, thus maintaining intracellular quality control over their lifetime [6,66]. In the RPE, LAP plays a necessary role in cell homeostasis through the optimal clearance of phagocytosed OS fragments; this supports (1) the visual cycle by recycling retinoids, (2) retinal metabolism (e.g., by metabolizing lipids to generate ketones and thus providing energy to the neural retina), and by producing insulin locally to support homeostasis, (3) RPE and retinal health and function by preventing buildup of excess lipids, (4) ensuring the synthesis of anti-inflammatory lipids [11,28,30,43,67]. LAP thus serves a protective role in the retina. We have previously established that the LC3b, an LC3 isoform, plays a crucial role in RPE-LAP; it is critical for lipid homeostasis and in regulating the inflammatory state of the retina/RPE [5,28,41]. Here, using RNAseq based comparative transcriptomics, we identified 1533 DEGs with ~73% of these upregulated and 27% downregulated in the *LC3b*$^{-/-}$ RPE. There was no compensatory upregulation of any other Atg8/LC3 family members-*LC3a, Gabarap, Gabarapl1*, and *Gabarapl2*, consistent with previous studies showing no upregulation of *LC3a* in *LC3b*$^{-/-}$ [5,28,39,41,68]. In the absence of LC3b, inflammatory and complement-related pathways are upregulated while fatty acid metabolism, oxidative phosphorylation, and peroxisome pathways are downregulated. To the best of our knowledge, this is the first report using RNAseq based expression profiling in a defective LAP model.

3.1. LC3b and Lipid Metabolic Dysregulation

Daily phagocytosis of OS presents a unique set of challenges for the RPE; estimates suggest that each RPE processes ~0.08–0.15 pmoles of OS derived fatty acid per day [6,27,35]. Excessive lipid accumulation and formation of lipid-peroxidation adducts in RPE/Ch is a common feature of mouse models of defective phagosome transport and degradation [30,56,69]. The RPE utilizes LAP in the daily ingestion of lipids that it degrades to provide metabolic intermediates; the lipids provide a critical energy source for the RPE through fatty acid oxidation and metabolically couple with photoreceptors to provide β-hydroxybutyrate (β-HB) [35,36,42].

Herein, we found that the hallmark pathways for oxidative phosphorylation and fatty acid metabolism are significantly downregulated in 24-month-old old *LC3b*$^{-/-}$ mice. Leading-edge gene subsets of these pathways include *Acadvl, Cpt2, Cpt1a*, and *Acadl* (involved in mitochondrial fatty acid β-oxidation), *Sdhc, Sdha, Sdhd, Aco2, Suclg1* (involved in TCA cycle), and *Hmgcs2* (rate limiting enzyme in ketogenesis). Approximately 30% of OS lipids are very long chain fatty acids (VLCFAs, C $\geq$ 20), which are preferentially catabolized in peroxisomes via β-oxidation [53,54]. Therefore, efficient lipid catabolism in the RPE requires the coordination of β-oxidation pathways within both mitochondria and peroxisomes [42,53,54,70]. Our GSEA analysis showed significant downregulation of peroxisome pathways, both biogenesis and turnover, as indicated by alterations in *Acox1* and *Cat*, as well as *Pex6*, *Pex11a*, and *Pex2*. The protein products of the Acox gene family, the acyl-CoA oxidases (ACOXs) catalyze desaturation of the AcylCoA esters in the committed step of peroxisome fatty acid oxidation [53,54]. Hydrogen peroxide generated in the ACOX reaction is rapidly degraded by the anti-oxidant enzyme catalase in a coupled reaction. Peroxisomes are the main site for catalase dependent antioxidant activity to maintain redox homeostasis of the RPE [71]. In the RPE, peroxisome turnover is an LC3b dependent process; *LC3b*$^{-/-}$ RPE have elevated peroxisome numbers with reduced antioxidant function reminiscent of aging/disease RPE [42,71,72]. Furthermore, peroxisome catalase activity is lower in primary RPE from aged donors and those with AMD [73]. While the interplay between LAP, peroxisome FAO and peroxisome turnover is a subject of future investigation; the downregulation of the hallmark peroxisome pathway in the *LC3b*$^{-/-}$ further lends support to decline in peroxisome function contributing to lipid dysregulation, higher oxidative stress, and disease pathogenesis.

Mitochondrial ketogenesis often serves as a fat disposal conduit, specifically when fatty acid oxidation exceeds mitochondrial capacity [37,74]. Such decreased capability may be due to mitochondrial dysfunction, aging, or disease [75], as well as lipid overload (for example, after a high fat meal). By disposing of acetyl-CoA, a product of FAO, ketogenesis prevents the need for terminal oxidation through the TCA cycle thus decreasing oxidative stress due to enhanced TCA flux [76]. Progressive mitochondrial dysfunction is a major contributor to the pathophysiology of age-related diseases of the outer retina [55,77,78]. Mice lacking *Hmgcs2* exhibited ketogenic deficiency and develop non-alcoholic fatty liver disease spontaneously [79]. *RetSat*, coding for retinol saturase, an oxidoreductase with diverse functions, including retinoid metabolism, was also included in the leading edge gene subsets. In adipocytes, *RetSat* expression is regulated by PPAR γ and is proposed to be involved in insulin sensitivity [80,81]. *Retsat*$^{-/-}$ mice show reduced production of all-trans-13,14-dihy-droretinol from dietary vitamin A, an increased accumulation of neutral lipids, and increased adiposity [80,82].

Our transcriptomic analysis provided unique insight into the regulation of metabolic pathways at the level of gene expression in RPE-LAP deficient cells. Although fatty acid metabolism and oxidative phosphorylation pathways were down regulated, cholesterol homoeostasis pathways were upregulated. The RPE not only synthesizes cholesterol through the mevalonate pathway, but also takes up cholesterol from the circulation, as well as the daily phagocytosis of OS tips with cholesterol homeostasis regulated via cholesterol efflux [83–85]. In the aging macula, dysregulation of cholesterol metabolism and lipoprotein processing are considered contributors to the onset and development of age-related degeneration [56]. Non-alcoholic fatty liver disease is similarly associated with dysregulated cholesterol metabolism, and it manifests on a molecular level as cholesterol accumulation in the mitochondria [86]. Schirris and colleagues [87], using metabolic network modeling, suggest cholesterol biosynthesis as a potential compensatory pathway in mitochondrial dysfunction serving as a means by which to restore the NADH and NADPH balance. Our own transcriptomic studies (Figures 5D and S2A) and previous in vitro studies suggest mitochondrial dysfunction in LAP-deficient RPE [88]. If compensatory, cholesterol biosynthesis as a means to maintain homeostasis presents a unique challenge to the RPE, as cholesterol is also taken up through daily the LAP-dependent degradation of OS tips, the loss of which results in high levels of the pro-inflammatory sterol, 7-keto cholesterol, a component of AMD-associated drusen [89].

A critical aspect of cholesterol efflux in the RPE is cholesterol esterification and subsequent packaging and secretion in lipoprotein-like particles (LLP) by the RPE back to the circulation [56]. These lipoproteins called BrM-LLP are distinct from circulating plasma lipoproteins [90]; esterified cholesterol is the largest component of BrM-LLP, it is over 10-fold more abundant than triglyceride [91]. Our transcriptomic analyses highlights modulation of numerous genes associated with lipoprotein metabolism, including *ApoO*, *Pltp*, *Mttp*, *ApoC4*, and *ApoA2* all of which are downregulated. As a group these genes are associated with plasma lipoprotein assembly, remodeling, and clearance. Of note, *Mttp*, encoding for microsomal transfer protein is necessary for the synthesis of β-lipoproteins, likely BrM-LLP by the RPE [55,90,92]. Interestingly, two genes, *ApoBec1* and *ApoBec3*, involved in apolipoprotein B mRNA editing, are both upregulated. What role this gene editing activity plays in RPE-specific β-lipoproteins assembly is unknown. Further studies are necessary to understand how cholesterol biosynthesis and packaging in lipoproteins is influenced by LAP with an emphasis on therapeutics designed to restore lipid homeostasis [57].

The metabolic fate of tissues is not only regulated by the levels of rate-limiting metabolic enzymes, but also by the expression and localization of solute transporters. Glucose is the primary metabolic substrate of the neural retina and is transported from the choroidal blood supply to the outer retina by GLUT1 (*Slc2al*) transporters in the apical and basolateral membranes of the RPE. The lactate generated in the outer retina through aerobic glycolysis is transported out of the retina by lactate transporters expressed in the apical (MCT1) and basolateral (MCT3) membranes of the RPE [93,94]. We found the genes encod-

ing these transporters (*Slc2a1*, *Slc16a1*, and Slc16a8) were all decreased in the *LC3b*$^{-/-}$ RPE (Figure 6A). Previous studies have shown MCT3 expression is reduced by mitochondrial dysfunction and RPE atrophy [95]. Furthermore, *SLC16a8* (MCT3) is a risk allele for AMD, and the loss of MCT3 expression was observed at early stages of AMD [96,97]. The reduced MCT3 expression in the *LC3b*$^{-/-}$ RPE is consistent with previous findings, showing that the expression of RPE signature genes are impacted by mitochondrial dysregulation and inflammation [98].

3.2. Defective LAP, Inflammation, and Complement System

Progress in understanding LAP in professional and specialized phagocytes has shown some interesting parallels. In macrophages and other immune cells, defective LAP leads to increased inflammatory signaling and inflammatory cytokine production [3,99,100]. RPE cells are one of the "most oxidative environments" in the body [101,102], generating reactive oxygen species resulting from an oxygen-rich environment, high metabolic activity, daily flux of polyunsaturated fatty acids due to OS phagocytosis, and bisretinoid accumulation [6,103,104]. Chronic oxidative stress contributes to numerous retinal degenerative diseases, including AMD [105,106]. In the absence of LC3b, undigested lipids act as substrates for lipid peroxidation reactions; there is an accumulation of the proinflammatory sterol, 7-ketocholesterol (7KCh), and reduced biosynthesis of anti-inflammatory molecules—NPD1 and maresin-1—thus further exacerbating inflammation [24,28,107,108]. Our GSEA analyses show that inflammatory and complement pathways are significantly upregulated in the *LC3b*$^{-/-}$, potentially contributing to an AMD-like phenotype. Polymorphisms in complement factor genes in the context of environmental risk factors are associated with AMD [109–111]. Several studies point to an intimate relationship between oxidative stress, complement activation, and inflammation in models of AMD [56,109,112–115]. Moreover, in an in vitro RPE lipid steatosis model, in which the loss of the autophagy protein, LC3b, results in defective phagosome degradation and metabolic dysregulation, we show that lipid overload results in increased gasdermin cleavage, IL-1β release, lipid accumulation, and decreased oxidative capacity [88]. The current RNAseq analyses expands these in vitro studies, as numerous cytokines and caspases (inflammatory response) are associated with the GSEA leading edge gene subsets in *LC3b*$^{-/-}$ RPE (see Figures 5A and S1A).

3.3. Lapses in LAP and AMD Associated Phenotype

Lipid metabolic imbalance is a hallmark of cardiovascular diseases, type 2 diabetes, Alzheimer's disease and AMD [116–122]. Moreover, several age-related disorders, including neurodegenerative disorders and AMD are associated with dysregulated autophagy [123]. Defects in autophagy and associated processes in long-lived post-mitotic cells like RPE that are challenged with lipid-rich OS throughout life makes them especially vulnerable to age-related pathologies [11,28,69]. A recent study on a cohort of Finnish patients reported several SNPs in the autophagy related genes, including rs73105013-T for *MAP1LC3A* that are associated with increased risk for wet AMD [124]. With a range of structural, metabolic, and functional defects, especially with regards to lipid dysregulation and inflammation, *LC3b*$^{-/-}$ RPE offers an opportunity to investigate the AMD-like phenotype in a mouse model. Using the comparative transcriptomics approach, here, we identified 8 DEGs overlapping with a list of prioritized genes associated with independent genetic signals in the largest AMD GWAS published to date [38,61]. These include: *Htra1*, *Tnfrsf10b*, *Tgfbr1*, *Trpm3*, *Tspan10*, *Slc16a8*, *Adamts9*, and *Rdh5* (mouse orthologs). Four of these genes: *Tspan10*, *Tnfrsf10b*, *Htra1*, and *Rdh5* also overlapped with a list of putative causal genes for AMD based on human eye eQTL (expression quantitative trait loci) and GWAS signal co-localization [125]. There is ongoing research in the field to investigate AMD pathogenesis using a range of approaches, such as gene expression studies on post-mortem eyes from AMD patients, in vitro studies with iPSC-RPE cells from subjects carrying risk allele variants, and animal models [126]. iPSCS-RPE cells derived from a patient carrying two copies of *SLC16A8* risk allele (rs77968014-G) showed deficit in transepithelial lactate

transport [127]. Furthermore, there was a progressive loss of MCT3 with an increasing severity of dry AMD [96]. An increase in the expression of HTRA1 protein was reported in iPSC-RPE cell line from subjects carrying a high-risk genotype at 10q26 locus [65,128], and a clinical trial evaluating the inhibition of HTRA1 is ongoing [129]. Mutations in *RDH5* have been reported in a subset of patients with macular atrophy [63,130]. A variant in *RDH5* has been shown to be associated with an increased skipping of exon 3, nonsense-mediated decay of the of aberrant transcript, and lower minor allele specific expression, thus providing a potential mechanistic link by which *RDH5* allele contributes to AMD risk [64]. Interestingly, expression of both *RDH5* and *TRPM3* decreases under inflammatory conditions in vitro and has been suggested to contribute to RPE dysfunction in AMD [131,132]. *TRPM3* codes for a calcium permeable cation channel activated by noxious heat, neurosteroid pregnenolone sulfate, or osmotic pressure [131–134]. *TRPM3* gene hosts *miR-204*, a microRNA highly expressed in the RPE that plays an important role in gene regulation and retinal/RPE homeostasis [134–136]. Furthermore, cholesterol enrichment inhibits TRPM3 activation and has been suggested as a mechanism for proinflammatory cytokine secretion associated with atherosclerotic processes [137]. Modulation of *Trpm3* levels along with cholesterol accumulation and increased inflammation observed in the *LC3b*$^{-/-}$ mouse RPE offers potential mechanistic insights into AMD pathogenesis [28]. Downregulation of *Trpm3* may also reduce inflammatory thermal hyperalgesia as has been seen in *Trpm3*$^{-/-}$ mice [138,139]. The RNAseq data using the *LC3b*$^{-/-}$ mouse model reported here is a valuable addition to bridge the gaps in our understanding of AMD pathophysiology and to identify potential therapeutic targets, and it has the potential to be extended to other lipid metabolic defects/age-related diseases as well.

4. Materials and Methods

4.1. Animals

LC3b$^{-/-}$ mice (strain name: B6;129P2-*Map1Lc3btm1Mrab*/J; stock # 009336 [68]) and C57BL6/J wildtype (WT) mice were purchased from Jackson Laboratory (Bar Harbor, ME, USA). The mouse lines were confirmed to be free of the *rd8* mutation by Transnetyx (Cordova, TN, USA). Maintenance of mouse colonies and all experiments involving animals were as described previously [12]. Mice were housed under standard cyclic light conditions: 12 h light/12 h dark and fed ad libitum, with both female and male mice used in these studies. All procedures involving animals were approved by the Institutional Animal Care and Use Committees (IACUC) of the University of Pennsylvania and were in accordance with the Association for Research in Vision and Ophthalmology (ARVO) guidelines for use of animals in research.

4.2. Antibodies

Primary antibodies used were: mouse anti-β-Actin (A2228; Sigma-Aldrich, St. Louis, MO, USA), goat anti-p-cadherin (AF761, R&D Systems, Minneapolis, MN, USA), rabbit anti-MCT3 [140], rabbit-anti-GAPDH (#5174, Cell Signaling Technology, Danvers, MA, USA), and mouse anti-RPE65 (NB100-355, Novus Biologicals LLC, Centennial, CO, USA). Secondary antibodies used were: goat anti-mouse and goat anti-rabbit horseradish peroxidase (HRP)-conjugated antibodies (Thermo Fisher Scientific, Waltham, MA, USA), donkey anti-goat, and anti-rabbit IgG Alexa Fluor 594/488 conjugates (Invitrogen, Waltham, MA, USA).

4.3. RPE Cell Isolation

RPE cells from WT (N = 4) and the *LC3b*$^{-/-}$ (N = 3) mice (age ~24 months) eyes were isolated with enzymatic treatment and gentle dissociation as described [141] with minor modifications. Briefly, the mice were anesthetized by CO_2 asphyxiation, the eyes were enucleated, and muscles and connective tissue were removed in ice cold HBSS-H− (HBSS without calcium or magnesium + 10 mM HEPES). Cornea, ciliary body, and lens were removed, and the eyecups were incubated in 1mg/mL Hyaluronidase solution (in

HBSS-H−) at 37 °C, 5% CO_2 for 20 min followed by incubation in ice-cold HBSS-H+ (HBSS with calcium and magnesium + 10 mM HEPES) and gently pulling away the neural retina. Next, the RPE/choroid was incubated in 0.25% trypsin at 37 °C, 5% CO_2 for 1 h, transferred to 20% fetal bovine serum (FBS) /HBSS-H+ solution, and gently shaken to detach RPE sheets, followed by centrifugation at 240× *g* for 5 min to collect the RPE sheets/cells.

4.4. RNA Isolation and Library Preparation

Total RNA was isolated with RNAEasy Plus Mini kit (QIAgen, Hilden, Germany) per manufacturer's instructions. RNA concentration, and sample quality was determined using an Agilent bioanalyzer. Total RNA samples with a RIN value of 7.1 (+/− 0.29) and a concentration between 1.1 and 2.7 ng/µL were used. An amount of 15 ng of total RNA were used for library preparation using NEB Ultra II stranded mRNA library kit (New England Biolabs, Ipswich, MA, USA) as per manufacturer's instructions and assessed for quality. Libraries were subjected to 100 bp single read sequencing on a NovaSeq SP flow cell using a NovaSeq 6000 sequencing system (Illumina, San Diego, CA, USA) by the Next-Generation Sequencing Core of the University of Pennsylvania. The raw RNAseq data has been deposited in the Gene Expression Omnibus database (GEO, NCBI) under the accession number GSE225344.

4.5. RNAseq Data Analysis

Fastq files containing raw data were imported into Salmon (v1.9.0) [142] to count hits against the transcriptome defined in Gencode (vM26) (annotation built on genome assembly GRCm39) [143]. Further analysis was done using several bioconductor packages in R (v4.2.2). The transcriptome count data was annotated and summarized to the gene level with tximeta (v1.16.1) [144] and further annotated with biomaRt (v2.54.1) [145]. Principal Component Analysis (PCA) coordinates were calculated with the bioconductor (v3.16) package PCAtools (v2.10.0). The normalizations and statistical analyses were done with DESeq2 (v1.38.3) [144].

4.6. Enrichment Analysis

DESeq2 was used to determine the significance of differential expression between the two groups. Genes showing a fold change of ≤ -1.5 or ≥ 1.5 (Log2-transformed ratio of ≤ -0.585 or ≥ 0.585), and an adjusted *p*-value (*p*-value corrected for false discovery rate using Benjamini-Hochberg method) ≤ 0.05 was considered significantly differentially expressed genes (DEGs). The up- and downregulated DEGs were tested for enrichment of Gene Ontology (GO) pathways using Metascape [146]. Additionally, an unfiltered list of genes ranked by their DESeq2 statistic was analyzed with GSEA (Gene Set Enrichment Analysis, v4.3.2), where pre-ranked analyses against gene collections in the Molecular Signatures Database (MSigDB, v2022.1.Hs) were carried out [147,148]. Enrichment scores and statistics for genesets in the hallmark collection were calculated.

4.7. Gene Expression Visualization

Variance stabilized expression values (calculated with DESeq2) for DEGs were used to generate heatmaps using the ClustVis web tool [149]. Rows were clustered using correlation distance and average linkage. Volcano plot was constructed using VolcaNoseR webapp using log2Fold change on the X axis and −log10(adjusted P) on the Y axis [150,151].

4.8. Protein–Protein Interaction Network Analysis

STRING database (version 11.5) was used to predict protein-protein interactions network (PPI) with cutoff criterion score >0.4; interaction sources included text-mining, experiments, and curated databases [152,153].

4.9. Immunoblotting

Immunoblotting was performed as described previously [28]. Cleared RPE and retinal lysates were prepared in RIPA buffer with 1% protease inhibitor mixture (Sigma-Aldrich, Burlington, MA, USA; P8340) and 2% phosphatase inhibitor mixture 2 (Sigma-Aldrich; P5726). 10–15 µg of protein was separated on 12% Bis-Tris-PAGE (Invitrogen) under reducing conditions and transferred to PVDF membranes (Millipore, Billerica, MA, USA). Membranes were blocked with 5% milk in PBS, 0.1% Tween-20 for 1 h at room temperature and incubated with primary antibodies for anti-MCT3 (1:5000), anti-GAPDH (1:10,000), anti-RPE65 (1:1000), or anti-β-actin (1:5000) overnight at 4 °C. Membranes were washed and incubated with goat anti-rabbit (1:3000) or goat anti-mouse (1:3000) HRP-conjugated secondary antibodies for 1 h at room temperature. The blots were developed using ECL SuperSignal® West Dura extended duration substrate (Thermo Scientific) and captured on Odyssey Fc (LI-COR Biosciences, Lincoln, NE, USA) and quantified as described [35].

4.10. Immunostaining

Immunostaining was performed on RPE/choroid flat mounts [28]. An amount of ~24-month-old WT and *LC3b*$^{-/-}$ mice were anesthetized, and the eyes were enucleated and incised just below the ora serrata. RPE/choroid flat-mounts were prepared by separating the retina from the RPE followed by fixation in 4% PFA for 30 min at room temp. Flat-mounts were permeabilized and blocked in blocking solution containing 5% BSA in PBS + 0.2% Triton X-100 (PBST) at 37 °C for 1 h, incubated with primary antibody diluted in blocking solution (1:2000 for rabbit anti-MCT3 or 1:200 for goat P-cadherin) at 4 °C overnight, washed three times with PBST, incubated in appropriate secondary antibodies conjugated to Alexa Fluor dyes (Invitrogen, Donkey anti-rabbit 488 + donkey anti-goat 594; 1:1000), and Hoechst 33258 (1:10,000) at 37 °C for 1 h and washed three times. Flat-mounts were mounted in Prolong Gold (Invitrogen). Images were captured on a Nikon A1R laser scanning confocal microscope with a PLAN APO VC 60× water (NA 1.2) objective at 18 °C, and the data were analyzed using Nikon Elements AR 4.30.01 software.

4.11. Statistical Analysis

Gene level statistical tests were done using DESeq2 and pathway enrichment statistical tests were done using GSEA and Metascape. List overlaps were analyzed using the Chi squared ($\chi 2$) test of independence using GraphPad. A 2-tailed *p*-value was computed.

Supplementary Materials: The following supporting information can be downloaded at: https://www.mdpi.com/article/10.3390/ijms24076716/s1.

Author Contributions: Conceptualization, K.B-B.; methodology, A.D. and J.W.T.; formal analysis, A.D., J.W.T. and K.B.-B.; investigation, K.B.-B. and N.J.P.; data curation, A.D. and J.W.T.; writing—original draft preparation, A.D.; writing—review and editing, J.W.T., K.B.-B. and N.J.P.; supervision, K.B.-B.; project administration, K.B.-B. and N.J.P.; funding acquisition, K.B.-B. and N.J.P. All authors have read and agreed to the published version of the manuscript.

Funding: This research was funded by the National Institute of Health NEI-EY-026525 (KBB and NJP), NEI-EY-032743 (KBB and MMH) and NEI core grant (P30 EY001583).

Institutional Review Board Statement: All procedures involving animals were approved by the Institutional Animal Care and Use Committees (IACUC) of the University of Pennsylvania and were in accordance with the Association for Research in Vision and Ophthalmology (ARVO) guidelines for use of animals in research.

Informed Consent Statement: Not applicable.

Data Availability Statement: The raw RNAseq data has been deposited in the Gene Expression Omnibus database (GEO, NCBI) under the accession number GSE225344.

Acknowledgments: We thank Penn Genomics Analysis Core for support with RNAseq analyses, and PDM-Live Cell Imaging Core (University of Pennsylvania) for imaging and analyses. We thank Rachel C. Sharp and Lauren Daniele for their support with the immunoblotting experiments.

Conflicts of Interest: The authors declare no conflict of interest. The funders had no role in the design of the study; in the collection, analyses, or interpretation of data; in the writing of the manuscript; or in the decision to publish the results.

References

1. Dikic, I.; Elazar, Z. Mechanism and medical implications of mammalian autophagy. *Nat. Rev. Mol. Cell Biol.* **2018**, *19*, 349–364. [CrossRef]
2. Cemma, M.; Brumell, J.H. Interactions of pathogenic bacteria with autophagy systems. *Curr. Biol.* **2012**, *22*, R540–R545. [CrossRef]
3. Peña-Martinez, C.; Rickman, A.D.; Heckmann, B.L. Beyond autophagy: LC3-associated phagocytosis and endocytosis. *Sci. Adv.* **2022**, *8*, eabn1702. [CrossRef]
4. Ohsumi, Y. Historical landmarks of autophagy research. *Cell Res.* **2014**, *24*, 9–23. [CrossRef]
5. Klionsky, D.J.; Abdel-Aziz, A.K.; Abdelfatah, S.; Abdellatif, M.; Abdoli, A.; Abel, S.; Abeliovich, H.; Abildgaard, M.H.; Abudu, Y.P.; Acevedo-Arozena, A.; et al. Guidelines for the use and interpretation of assays for monitoring autophagy (4th edition)(1). *Autophagy* **2021**, *17*, 1–382. [CrossRef] [PubMed]
6. Liton, P.B.; Boesze-Battaglia, K.; Boulton, M.E.; Boya, P.; Ferguson, T.A.; Ganley, I.G.; Kauppinnen, A.; Laurie, G.W.; Mizushima, N.; Morishita, H.; et al. Autophagy in the Eye: From Physiology to Pathophysology. *Autophagy Rep.* **2023**, *2*, 2178996. [CrossRef]
7. Xie, Y.; Li, J.; Kang, R.; Tang, D. Interplay Between Lipid Metabolism and Autophagy. *Front. Cell Dev. Biol.* **2020**, *8*, 431. [CrossRef]
8. Heckmann, B.L.; Green, D.R. LC3-associated phagocytosis at a glance. *J. Cell Sci.* **2019**, *132*, jcs222984. [CrossRef] [PubMed]
9. Grijmans, B.J.M.; van der Kooij, S.B.; Varela, M.; Meijer, A.H. LAPped in Proof: LC3-Associated Phagocytosis and the Arms Race Against Bacterial Pathogens. *Front. Cell. Infect. Microbiol.* **2021**, *11*, 809121. [CrossRef] [PubMed]
10. Asare, P.F.; Tran, H.B.; Hurtado, P.R.; Perkins, G.B.; Nguyen, P.; Jersmann, H.; Roscioli, E.; Hodge, S. Inhibition of LC3-associated phagocytosis in COPD and in response to cigarette smoke. *Adv. Respir. Dis.* **2021**, *15*, 17534666211039769. [CrossRef]
11. Kim, J.Y.; Zhao, H.; Martinez, J.; Doggett, T.A.; Kolesnikov, A.V.; Tang, P.H.; Ablonczy, Z.; Chan, C.C.; Zhou, Z.; Green, D.R.; et al. Noncanonical autophagy promotes the visual cycle. *Cell* **2013**, *154*, 365–376. [CrossRef]
12. Frost, L.S.; Lopes, V.S.; Bragin, A.; Reyes-Reveles, J.; Brancato, J.; Cohen, A.; Mitchell, C.H.; Williams, D.S.; Boesze-Battaglia, K. The Contribution of Melanoregulin to Microtubule-Associated Protein 1 Light Chain 3 (LC3) Associated Phagocytosis in Retinal Pigment Epithelium. *Mol. Neurobiol.* **2015**, *52*, 1135–1151. [CrossRef]
13. Yefimova, M.G.; Ravel, C.; Rolland, A.D.; Bourmeyster, N.; Jégou, B. MERTK-Mediated LC3-Associated Phagocytosis (LAP) of Apoptotic Substrates in Blood-Separated Tissues: Retina, Testis, Ovarian Follicles. *Cells* **2021**, *10*, 1443. [CrossRef] [PubMed]
14. Panneerdoss, S.; Viswanadhapalli, S.; Abdelfattah, N.; Onyeagucha, B.C.; Timilsina, S.; Mohammad, T.A.; Chen, Y.; Drake, M.; Vuori, K.; Kumar, T.R.; et al. Cross-talk between miR-471-5p and autophagy component proteins regulates LC3-associated phagocytosis (LAP) of apoptotic germ cells. *Nat. Commun.* **2017**, *8*, 598. [CrossRef]
15. Green, D.R.; Levine, B. To be or not to be? How selective autophagy and cell death govern cell fate. *Cell* **2014**, *157*, 65–75. [CrossRef] [PubMed]
16. Martinez, J.; Almendinger, J.; Oberst, A.; Ness, R.; Dillon, C.P.; Fitzgerald, P.; Hengartner, M.O.; Green, D.R. Microtubule-associated protein 1 light chain 3 alpha (LC3)-associated phagocytosis is required for the efficient clearance of dead cells. *Proc. Natl. Acad. Sci. USA* **2011**, *108*, 17396–17401. [CrossRef]
17. Minami, S.; Nakamura, S.; Yoshimori, T. Rubicon in Metabolic Diseases and Ageing. *Front. Cell Dev. Biol.* **2022**, *9*, 3798. [CrossRef]
18. Martinez, J.; Malireddi, R.K.; Lu, Q.; Cunha, L.D.; Pelletier, S.; Gingras, S.; Orchard, R.; Guan, J.L.; Tan, H.; Peng, J.; et al. Molecular characterization of LC3-associated phagocytosis reveals distinct roles for Rubicon, NOX2 and autophagy proteins. *Nat. Cell Biol.* **2015**, *17*, 893–906. [CrossRef]
19. Ryter, S.W.; Lam, H.C.; Chen, Z.H.; Choi, A.M. Deadly triplex: Smoke, autophagy and apoptosis. *Autophagy* **2011**, *7*, 436–437. [CrossRef]
20. Kesireddy, V.S.; Chillappagari, S.; Ahuja, S.; Knudsen, L.; Henneke, I.; Graumann, J.; Meiners, S.; Ochs, M.; Ruppert, C.; Korfei, M.; et al. Susceptibility of microtubule-associated protein 1 light chain 3beta (MAP1LC3B/LC3B) knockout mice to lung injury and fibrosis. *FASEB J.* **2019**, *33*, 12392–12408. [CrossRef] [PubMed]
21. Asare, P.F.; Roscioli, E.; Hurtado, P.R.; Tran, H.B.; Mah, C.Y.; Hodge, S. LC3-Associated Phagocytosis (LAP): A Potentially Influential Mediator of Efferocytosis-Related Tumor Progression and Aggressiveness. *Front. Oncol.* **2020**, *10*, 1298. [CrossRef]
22. Cunha, L.D.; Yang, M.; Carter, R.; Guy, C.; Harris, L.; Crawford, J.C.; Quarato, G.; Boada-Romero, E.; Kalkavan, H.; Johnson, M.D.L.; et al. LC3-Associated Phagocytosis in Myeloid Cells Promotes Tumor Immune Tolerance. *Cell* **2018**, *175*, 429–441. [CrossRef]
23. Martinez, J. LAP it up, fuzz ball: A short history of LC3-associated phagocytosis. *Curr. Opin. Immunol.* **2018**, *55*, 54–61. [CrossRef] [PubMed]
24. Wang, L.; Chen, P.; Xiao, W. β-hydroxybutyrate as an Anti-Aging Metabolite. *Nutrients* **2021**, *13*, 3420. [CrossRef]

25. Yang, S.; Zhou, J.; Li, D. Functions and Diseases of the Retinal Pigment Epithelium. *Front. Pharmacol.* **2021**, *12*, 727870. [CrossRef] [PubMed]
26. Kevany, B.M.; Palczewski, K. Phagocytosis of retinal rod and cone photoreceptors. *Physiology* **2010**, *25*, 8–15. [CrossRef] [PubMed]
27. Volland, S.; Esteve-Rudd, J.; Hoo, J.; Yee, C.; Williams, D.S. A comparison of some organizational characteristics of the mouse central retina and the human macula. *PLoS ONE* **2015**, *10*, e0125631. [CrossRef]
28. Dhingra, A.; Bell, B.A.; Peachey, N.S.; Daniele, L.L.; Reyes-Reveles, J.; Sharp, R.C.; Jun, B.; Bazan, N.G.; Sparrow, J.R.; Kim, H.J.; et al. Microtubule-Associated Protein 1 Light Chain 3B, (LC3B) Is Necessary to Maintain Lipid-Mediated Homeostasis in the Retinal Pigment Epithelium. *Front. Cell. Neurosci.* **2018**, *12*, 351. [CrossRef]
29. Strauss, O. The Retinal Pigment Epithelium in Visual Function. *Physiol. Rev.* **2005**, *85*, 845–881. [CrossRef]
30. Zhang, Y.; Cross, S.D.; Stanton, J.B.; Marmorstein, A.D.; Le, Y.Z.; Marmorstein, L.Y. Early AMD-like defects in the RPE and retinal degeneration in aged mice with RPE-specific deletion of Atg5 or Atg7. *Mol. Vis.* **2017**, *23*, 228–241. [PubMed]
31. Curcio, C.A.; Johnson, M.; Rudolf, M.; Huang, J.D. The oil spill in ageing Bruch membrane. *Br. J. Ophthalmol.* **2011**, *95*, 1638–1645. [CrossRef]
32. Malek, G.; Li, C.M.; Guidry, C.; Medeiros, N.E.; Curcio, C.A. Apolipoprotein B in cholesterol-containing drusen and basal deposits of human eyes with age-related maculopathy. *Am. J. Pathol.* **2003**, *162*, 413–425. [CrossRef] [PubMed]
33. Curcio, C.A.; Presley, J.B.; Millican, C.L.; Medeiros, N.E. Basal deposits and drusen in eyes with age-related maculopathy: Evidence for solid lipid particles. *Exp. Eye Res.* **2005**, *80*, 761–775. [CrossRef] [PubMed]
34. Chen, L.; Messinger, J.D.; Zhang, Y.; Spaide, R.F.; Freund, K.B.; Curcio, C.A. SUBRETINAL DRUSENOID DEPOSIT IN AGE-RELATED MACULAR DEGENERATION: Histologic Insights Into Initiation, Progression to Atrophy, and Imaging. *Retina* **2020**, *40*, 618–631. [CrossRef]
35. Reyes-Reveles, J.; Dhingra, A.; Alexander, D.; Bragin, A.; Philp, N.J.; Boesze-Battaglia, K. Phagocytosis-dependent ketogenesis in retinal pigment epithelium. *J. Biol. Chem.* **2017**, *292*, 8038–8047. [CrossRef]
36. Adijanto, J.; Du, J.; Moffat, C.; Seifert, E.L.; Hurle, J.B.; Philp, N.J. The retinal pigment epithelium utilizes fatty acids for ketogenesis. *J. Biol. Chem.* **2014**, *289*, 20570–20582. [CrossRef]
37. Cotter, D.G.; Ercal, B.; Huang, X.; Leid, J.M.; d'Avignon, D.A.; Graham, M.J.; Dietzen, D.J.; Brunt, E.M.; Patti, G.J.; Crawford, P.A. Ketogenesis prevents diet-induced fatty liver injury and hyperglycemia. *J. Clin. Investig.* **2014**, *124*, 5175–5190. [CrossRef]
38. Fritsche, L.G.; Igl, W.; Bailey, J.N.; Grassmann, F.; Sengupta, S.; Bragg-Gresham, J.L.; Burdon, K.P.; Hebbring, S.J.; Wen, C.; Gorski, M.; et al. A large genome-wide association study of age-related macular degeneration highlights contributions of rare and common variants. *Nat. Genet.* **2016**, *48*, 134–143. [CrossRef] [PubMed]
39. Lee, Y.K.; Lee, J.A. Role of the mammalian ATG8/LC3 family in autophagy: Differential and compensatory roles in the spatiotemporal regulation of autophagy. *BMB Rep.* **2016**, *49*, 424–430. [CrossRef] [PubMed]
40. Shpilka, T.; Weidberg, H.; Pietrokovski, S.; Elazar, Z. Atg8: An autophagy-related ubiquitin-like protein family. *Genome Biol.* **2011**, *12*, 226. [CrossRef]
41. Dhingra, A.; Alexander, D.; Reyes-Reveles, J.; Sharp, R.; Boesze-Battaglia, K. Microtubule-Associated Protein 1 Light Chain 3 (LC3) Isoforms in RPE and Retina. *Adv. Exp. Med. Biol.* **2018**, *1074*, 609–616. [CrossRef]
42. Daniele, L.L.; Caughey, J.; Volland, S.; Sharp, R.C.; Dhingra, A.; Williams, D.S.; Philp, N.J.; Boesze-Battaglia, K. Peroxisome turnover and diurnal modulation of antioxidant activity in retinal pigment epithelia utilizes microtubule-associated protein 1 light chain 3B (LC3B). *Am. J. Physiol. Cell Physiol.* **2019**, *317*, C1194–C1204. [CrossRef]
43. Lakkaraju, A.; Umapathy, A.; Tan, L.X.; Daniele, L.; Philp, N.J.; Boesze-Battaglia, K.; Williams, D.S. The cell biology of the retinal pigment epithelium. *Prog. Retin. Eye Res.* **2020**, *78*, 100846. [CrossRef] [PubMed]
44. Adijanto, J.; Philp, N.J. The SLC16A family of monocarboxylate transporters (MCTs)–physiology and function in cellular metabolism, pH homeostasis, and fluid transport. *Curr. Top. Membr.* **2012**, *70*, 275–311. [CrossRef] [PubMed]
45. Felmlee, M.A.; Jones, R.S.; Rodriguez-Cruz, V.; Follman, K.E.; Morris, M.E. Monocarboxylate Transporters (SLC16): Function, Regulation, and Role in Health and Disease. *Pharmacol. Rev.* **2020**, *72*, 466–485. [CrossRef] [PubMed]
46. Philp, N.J.; Ochrietor, J.D.; Rudoy, C.; Muramatsu, T.; Linser, P.J. Loss of MCT1, MCT3, and MCT4 expression in the retinal pigment epithelium and neural retina of the 5A11/basigin-null mouse. *Investig. Ophthalmol. Vis. Sci.* **2003**, *44*, 1305–1311. [CrossRef] [PubMed]
47. Han, J.Y.S.; Kinoshita, J.; Bisetto, S.; Bell, B.A.; Nowak, R.A.; Peachey, N.S.; Philp, N.J. Role of monocarboxylate transporters in regulating metabolic homeostasis in the outer retina: Insight gained from cell-specific Bsg deletion. *FASEB J.* **2020**, *34*, 5401–5419. [CrossRef] [PubMed]
48. Strunnikova, N.V.; Maminishkis, A.; Barb, J.J.; Wang, F.; Zhi, C.; Sergeev, Y.; Chen, W.; Edwards, A.O.; Stambolian, D.; Abecasis, G.; et al. Transcriptome analysis and molecular signature of human retinal pigment epithelium. *Hum. Mol. Genet.* **2010**, *19*, 2468–2486. [CrossRef]
49. Borooah, S.; Phillips, M.J.; Bilican, B.; Wright, A.F.; Wilmut, I.; Chandran, S.; Gamm, D.; Dhillon, B. Using human induced pluripotent stem cells to treat retinal disease. *Prog. Retin. Eye Res.* **2013**, *37*, 163–181. [CrossRef]
50. Calderon-Dominguez, M.; Gil, G.; Medina, M.A.; Pandak, W.M.; Rodriguez-Agudo, D. The StarD4 subfamily of steroidogenic acute regulatory-related lipid transfer (START) domain proteins: New players in cholesterol metabolism. *Int. J. Biochem. Cell Biol.* **2014**, *49*, 64–68. [CrossRef]

51. Watts, G.F.; Ding, P.Y.A.; George, P.; Hagger, M.S.; Hu, M.; Lin, J.; Khoo, K.L.; Marais, A.D.; Miida, T.; Nawawi, H.M.; et al. Translational Research for Improving the Care of Familial Hypercholesterolemia: The "Ten Countries Study" and Beyond. *J. Atheroscler. Thromb.* **2016**, *23*, 891–900. [CrossRef]
52. Wong, S.K.; Ramli, F.F.; Ali, A.; Ibrahim, N. Genetics of Cholesterol-Related Genes in Metabolic Syndrome: A Review of Current Evidence. *Biomedicines* **2022**, *10*, 3239. [CrossRef] [PubMed]
53. Schrader, M.; Costello, J.; Godinho, L.F.; Islinger, M. Peroxisome-mitochondria interplay and disease. *J. Inherit. Metab. Dis.* **2015**, *38*, 681–702. [CrossRef] [PubMed]
54. Van Veldhoven, P.P. Biochemistry and genetics of inherited disorders of peroxisomal fatty acid metabolism. *J. Lipid Res.* **2010**, *51*, 2863–2895. [CrossRef]
55. Handa, J.T.; Cano, M.; Wang, L.; Datta, S.; Liu, T. Lipids, oxidized lipids, oxidation-specific epitopes, and Age-related Macular Degeneration. *Biochim. Biophys. Acta (BBA)-Mol. Cell Biol. Lipids* **2017**, *1862*, 430–440. [CrossRef]
56. van Leeuwen, E.M.; Emri, E.; Merle, B.M.J.; Colijn, J.M.; Kersten, E.; Cougnard-Gregoire, A.; Dammeier, S.; Meester-Smoor, M.; Pool, F.M.; de Jong, E.K.; et al. A new perspective on lipid research in age-related macular degeneration. *Prog. Retin. Eye Res.* **2018**, *67*, 56–86. [CrossRef]
57. Landowski, M.; Bowes Rickman, C. Targeting Lipid Metabolism for the Treatment of Age-Related Macular Degeneration: Insights from Preclinical Mouse Models. *J. Ocul. Pharmacol. Ther.* **2022**, *38*, 3–32. [CrossRef]
58. Tan, L.X.; Germer, C.J.; La Cunza, N.; Lakkaraju, A. Complement activation, lipid metabolism, and mitochondrial injury: Converging pathways in age-related macular degeneration. *Redox Biol.* **2020**, *37*, 101781. [CrossRef]
59. Cherepanoff, S.; McMenamin, P.; Gillies, M.C.; Kettle, E.; Sarks, S.H. Bruch's membrane and choroidal macrophages in early and advanced age-related macular degeneration. *Br. J. Ophthalmol.* **2010**, *94*, 918–925. [CrossRef] [PubMed]
60. Tarallo, V.; Hirano, Y.; Gelfand, B.D.; Dridi, S.; Kerur, N.; Kim, Y.; Cho, W.G.; Kaneko, H.; Fowler, B.J.; Bogdanovich, S.; et al. DICER1 loss and Alu RNA induce age-related macular degeneration via the NLRP3 inflammasome and MyD88. *Cell* **2012**, *149*, 847–859. [CrossRef]
61. Strunz, T.; Kiel, C.; Sauerbeck, B.L.; Weber, B.H.F. Learning from Fifteen Years of Genome-Wide Association Studies in Age-Related Macular Degeneration. *Cells* **2020**, *9*, 2267. [CrossRef]
62. Daniele, L.L.; Sauer, B.; Gallagher, S.M.; Pugh, E.N., Jr.; Philp, N.J. Altered visual function in monocarboxylate transporter 3 (Slc16a8) knockout mice. *Am. J. Physiol. Cell Physiol.* **2008**, *295*, C451–C457. [CrossRef]
63. Occelli, L.M.; Daruwalla, A.; De Silva, S.R.; Winkler, P.A.; Sun, K.; Pasmanter, N.; Minella, A.; Querubin, J.; Lyons, L.A.; Consortium, L.; et al. A large animal model of RDH5-associated retinopathy recapitulates important features of the human phenotype. *Hum. Mol. Genet.* **2021**, *31*, 1263–1277. [CrossRef]
64. Liu, B.; Calton, M.A.; Abell, N.S.; Benchorin, G.; Gloudemans, M.J.; Chen, M.; Hu, J.; Li, X.; Balliu, B.; Bok, D.; et al. Genetic analyses of human fetal retinal pigment epithelium gene expression suggest ocular disease mechanisms. *Commun. Biol.* **2019**, *2*, 186. [CrossRef]
65. Lin, M.K.; Yang, J.; Hsu, C.W.; Gore, A.; Bassuk, A.G.; Brown, L.M.; Colligan, R.; Sengillo, J.D.; Mahajan, V.B.; Tsang, S.H. HTRA1, an age-related macular degeneration protease, processes extracellular matrix proteins EFEMP1 and TSP1. *Aging Cell* **2018**, *17*, e12710. [CrossRef] [PubMed]
66. Liang, Y.; Sigrist, S. Autophagy and proteostasis in the control of synapse aging and disease. *Curr. Opin. Neurobiol.* **2018**, *48*, 113–121. [CrossRef] [PubMed]
67. Iker Etchegaray, J.; Kelley, S.; Penberthy, K.; Karvelyte, L.; Nagasaka, Y.; Gasperino, S.; Paul, S.; Seshadri, V.; Raymond, M.; Marco, A.R.; et al. Phagocytosis in the retina promotes local insulin production in the eye. *Nat. Metab.* **2023**, *5*, 207–218. [CrossRef] [PubMed]
68. Cann, G.M.; Guignabert, C.; Ying, L.; Deshpande, N.; Bekker, J.M.; Wang, L.; Zhou, B.; Rabinovitch, M. Developmental expression of LC3alpha and beta: Absence of fibronectin or autophagy phenotype in LC3beta knockout mice. *Dev. Dyn.* **2008**, *237*, 187–195. [CrossRef] [PubMed]
69. Jiang, M.; Esteve-Rudd, J.; Lopes, V.S.; Diemer, T.; Lillo, C.; Rump, A.; Williams, D.S. Microtubule motors transport phagosomes in the RPE, and lack of KLC1 leads to AMD-like pathogenesis. *J. Cell Biol.* **2015**, *210*, 595–611. [CrossRef]
70. Fliesler, A.J.; Anderson, R.E. Chemistry and metabolism of lipids in the vertebrate retina. *Prog. Lipid Res.* **1983**, *22*, 79–131. [CrossRef]
71. Beier, K.; Völkl, A.; Fahimi, H.D. The impact of aging on enzyme proteins of rat liver peroxisomes: Quantitative analysis by immunoblotting and immunoelectron microscopy. *Virchows Arch. B Cell Pathol. Incl. Mol. Pathol.* **1993**, *63*, 139–146. [CrossRef] [PubMed]
72. Feher, J.; Kovacs, I.; Artico, M.; Cavallotti, C.; Papale, A.; Balacco Gabrieli, C. Mitochondrial alterations of retinal pigment epithelium in age-related macular degeneration. *Neurobiol. Aging* **2006**, *27*, 983–993. [CrossRef] [PubMed]
73. Liles, M.R.; Newsome, D.A.; Oliver, P.D. Antioxidant enzymes in the aging human retinal pigment epithelium. *Arch. Ophthalmol.* **1991**, *109*, 1285–1288. [CrossRef] [PubMed]
74. Cotter, D.G.; Schugar, R.C.; Crawford, P.A. Ketone body metabolism and cardiovascular disease. *Am. J. Physiol. Circ. Physiol.* **2013**, *304*, H1060–H1076. [CrossRef] [PubMed]
75. Wang, Y.; Grenell, A.; Zhong, F.; Yam, M.; Hauer, A.; Gregor, E.; Zhu, S.; Lohner, D.; Zhu, J.; Du, J. Metabolic signature of the aging eye in mice. *Neurobiol. Aging* **2018**, *71*, 223–233. [CrossRef] [PubMed]

76. d'Avignon, D.A.; Puchalska, P.; Ercal, B.; Chang, Y.; Martin, S.E.; Graham, M.J.; Patti, G.J.; Han, X.; Crawford, P.A. Hepatic ketogenic insufficiency reprograms hepatic glycogen metabolism and the lipidome. *J. Clin. Investig.* **2018**, *3*, e99762. [CrossRef]
77. Ferrington, D.A.; Ebeling, M.C.; Kapphahn, R.J.; Terluk, M.R.; Fisher, C.R.; Polanco, J.R.; Roehrich, H.; Leary, M.M.; Geng, Z.; Dutton, J.R.; et al. Altered bioenergetics and enhanced resistance to oxidative stress in human retinal pigment epithelial cells from donors with age-related macular degeneration. *Redox Biol.* **2017**, *13*, 255–265. [CrossRef] [PubMed]
78. Fisher, C.R.; Ferrington, D.A. Perspective on AMD Pathobiology: A Bioenergetic Crisis in the RPE. *Investig. Opthalmol. Vis. Sci.* **2018**, *59*, AMD41–AMD47. [CrossRef]
79. Asif, S.; Kim, R.Y.; Fatica, T.; Sim, J.; Zhao, X.; Oh, Y.; Denoncourt, A.; Cheung, A.C.; Downey, M.; Mulvihill, E.E.; et al. Hmgcs2-mediated ketogenesis modulates high-fat diet-induced hepatosteatosis. *Mol. Metab.* **2022**, *61*, 101494. [CrossRef]
80. Pang, X.Y.; Wang, S.; Jurczak, M.J.; Shulman, G.I.; Moise, A.R. Retinol saturase modulates lipid metabolism and the production of reactive oxygen species. *Arch. Biochem. Biophys.* **2017**, *633*, 93–102. [CrossRef]
81. Houten, S.M.; Violante, S.; Ventura, F.V.; Wanders, R.J.A. The Biochemistry and Physiology of Mitochondrial Fatty Acid β-Oxidation and Its Genetic Disorders. *Annu. Rev. Physiol.* **2016**, *78*, 23–44. [CrossRef]
82. Moise, A.R.; Lobo, G.P.; Erokwu, B.; Wilson, D.L.; Peck, D.; Alvarez, S.; Domínguez, M.; Alvarez, R.; Flask, C.A.; de Lera, A.R.; et al. Increased adiposity in the retinol saturase-knockout mouse. *FASEB J.* **2010**, *24*, 1261–1270. [CrossRef]
83. Pikuleva, I.A.; Curcio, C.A. Cholesterol in the retina: The best is yet to come. *Prog. Retin. Eye Res.* **2014**, *41*, 64–89. [CrossRef] [PubMed]
84. Buhaescu, I.; Izzedine, H. Mevalonate pathway: A review of clinical and therapeutical implications. *Clin. Biochem.* **2007**, *40*, 575–584. [CrossRef] [PubMed]
85. Fliesler, S.J.; Bretillon, L. The ins and outs of cholesterol in the vertebrate retina. *J. Lipid Res.* **2010**, *51*, 3399–3413. [CrossRef]
86. Solsona-Vilarrasa, E.; Fucho, R.; Torres, S.; Nuñez, S.; Nuño-Lámbarri, N.; Enrich, C.; García-Ruiz, C.; Fernández-Checa, J.C. Cholesterol enrichment in liver mitochondria impairs oxidative phosphorylation and disrupts the assembly of respiratory supercomplexes. *Redox Biol.* **2019**, *24*, 101214. [CrossRef]
87. Schirris, T.J.J.; Rossell, S.; de Haas, R.; Frambach, S.; Hoogstraten, C.A.; Renkema, G.H.; Beyrath, J.D.; Willems, P.; Huynen, M.A.; Smeitink, J.A.M.; et al. Stimulation of cholesterol biosynthesis in mitochondrial complex I-deficiency lowers reductive stress and improves motor function and survival in mice. *Biochim. et Biophys. Acta (BBA)-Mol. Basis Dis.* **2021**, *1867*, 166062. [CrossRef]
88. Dhingra, A.; Sharp, R.C.; Kim, T.; Popov, A.V.; Ying, G.S.; Pietrofesa, R.A.; Park, K.; Christofidou-Solomidou, M.; Boesze-Battaglia, K. Assessment of a Small Molecule Synthetic Lignan in Enhancing Oxidative Balance and Decreasing Lipid Accumulation in Human Retinal Pigment Epithelia. *Int. J. Mol. Sci.* **2021**, *22*, 5764. [CrossRef]
89. Wang, L.; Clark, M.E.; Crossman, D.K.; Kojima, K.; Messinger, J.D.; Mobley, J.A.; Curcio, C.A. Abundant lipid and protein components of drusen. *PLoS ONE* **2010**, *5*, e10329. [CrossRef] [PubMed]
90. Li, C.M.; Chung, B.H.; Presley, J.B.; Malek, G.; Zhang, X.; Dashti, N.; Li, L.; Chen, J.; Bradley, K.; Kruth, H.S.; et al. Lipoprotein-like particles and cholesteryl esters in human Bruch's membrane: Initial characterization. *Investig. Ophthalmol. Vis. Sci.* **2005**, *46*, 2576–2586. [CrossRef]
91. Wang, L.; Li, C.M.; Rudolf, M.; Belyaeva, O.V.; Chung, B.H.; Messinger, J.D.; Kedishvili, N.Y.; Curcio, C.A. Lipoprotein particles of intraocular origin in human Bruch membrane: An unusual lipid profile. *Investig. Opthalmology Vis. Sci.* **2009**, *50*, 870–877. [CrossRef]
92. Sirwi, A.; Hussain, M.M. Lipid transfer proteins in the assembly of apoB-containing lipoproteins. *J. Lipid Res.* **2018**, *59*, 1094–1102. [CrossRef] [PubMed]
93. Léveillard, T.; Philp, N.J.; Sennlaub, F. Is Retinal Metabolic Dysfunction at the Center of the Pathogenesis of Age-related Macular Degeneration? *Int. J. Mol. Sci.* **2019**, *20*, 762. [CrossRef]
94. Philp, N.J.; Wang, D.; Yoon, H.; Hjelmeland, L.M. Polarized expression of monocarboxylate transporters in human retinal pigment epithelium and ARPE-19 cells. *Investig. Opthalmol. Vis. Sci.* **2003**, *44*, 1716–1721. [CrossRef]
95. Adijanto, J.; Philp, N.J. Cultured primary human fetal retinal pigment epithelium (hfRPE) as a model for evaluating RPE metabolism. *Exp. Eye Res.* **2014**, *126*, 77–84. [CrossRef]
96. Vogt, S.D.; Curcio, C.A.; Wang, L.; Li, C.M.; McGwin, G., Jr.; Medeiros, N.E.; Philp, N.J.; Kimble, J.A.; Read, R.W. Retinal pigment epithelial expression of complement regulator CD46 is altered early in the course of geographic atrophy. *Exp. Eye Res.* **2011**, *93*, 413–423. [CrossRef]
97. Fritsche, L.G.; Chen, W.; Schu, M.; Yaspan, B.L.; Yu, Y.; Thorleifsson, G.; Zack, D.J.; Arakawa, S.; Cipriani, V.; Ripke, S.; et al. Seven new loci associated with age-related macular degeneration. *Nat. Genet.* **2013**, *45*, 433–439, 439e431–439e432. [CrossRef] [PubMed]
98. Zhao, C.; Yasumura, D.; Li, X.; Matthes, M.; Lloyd, M.; Nielsen, G.; Ahern, K.; Snyder, M.; Bok, D.; Dunaief, J.L.; et al. mTOR-mediated dedifferentiation of the retinal pigment epithelium initiates photoreceptor degeneration in mice. *J. Clin. Investig.* **2011**, *121*, 369–383. [CrossRef]
99. Tam, J.M.; Mansour, M.K.; Khan, N.S.; Seward, M.; Puranam, S.; Tanne, A.; Sokolovska, A.; Becker, C.E.; Acharya, M.; Baird, M.A.; et al. Dectin-1–Dependent LC3 Recruitment to Phagosomes Enhances Fungicidal Activity in Macrophages. *J. Infect. Dis.* **2014**, *210*, 1844–1854. [CrossRef] [PubMed]
100. Ma, J.; Becker, C.; Lowell, C.A.; Underhill, D.M. Dectin-1-triggered Recruitment of Light Chain 3 Protein to Phagosomes Facilitates Major Histocompatibility Complex Class II Presentation of Fungal-derived Antigens. *J. Biol. Chem.* **2012**, *287*, 34149–34156. [CrossRef]

101. Yu, D.-Y.; Cringle, S.J. Retinal degeneration and local oxygen metabolism. *Exp. Eye Res.* **2005**, *80*, 745–751. [CrossRef]
102. Trakkides, T.O.; Schäfer, N.; Reichenthaler, M.; Kühn, K.; Brandwijk, R.; Toonen, E.J.M.; Urban, F.; Wegener, J.; Enzmann, V.; Pauly, D. Oxidative Stress Increases Endogenous Complement-Dependent Inflammatory and Angiogenic Responses in Retinal Pigment Epithelial Cells Independently of Exogenous Complement Sources. *Antioxidants* **2019**, *8*, 548. [CrossRef]
103. Kim, H.J.; Montenegro, D.; Zhao, J.; Sparrow, J.R. Bisretinoids of the Retina: Photo-Oxidation, Iron-Catalyzed Oxidation, and Disease Consequences. *Antioxidants* **2021**, *10*, 1382. [CrossRef]
104. Asatryan, A.; Bazan, N.G. Molecular mechanisms of signaling via the docosanoid neuroprotectin D1 for cellular homeostasis and neuroprotection. *J. Biol. Chem.* **2017**, *292*, 12390–12397. [CrossRef] [PubMed]
105. Datta, S.; Cano, M.; Ebrahimi, K.; Wang, L.; Handa, J.T. The impact of oxidative stress and inflammation on RPE degeneration in non-neovascular AMD. *Prog. Retin. Eye Res.* **2017**, *60*, 201–218. [CrossRef]
106. Radu, R.A.; Hu, J.; Yuan, Q.; Welch, D.L.; Makshanoff, J.; Lloyd, M.; McMullen, S.; Travis, G.H.; Bok, D. Complement system dysregulation and inflammation in the retinal pigment epithelium of a mouse model for Stargardt macular degeneration. *J. Biol. Chem.* **2011**, *286*, 18593–18601. [CrossRef]
107. Vasconcelos, A.R.; Yshii, L.M.; Viel, T.A.; Buck, H.S.; Mattson, M.P.; Scavone, C.; Kawamoto, E.M. Intermittent fasting attenuates lipopolysaccharide-induced neuroinflammation and memory impairment. *J. Neuroinflamm.* **2014**, *11*, 85. [CrossRef]
108. Youm, Y.-H.; Nguyen, K.Y.; Grant, R.W.; Goldberg, E.L.; Bodogai, M.; Kim, D.; D'Agostino, D.; Planavsky, N.; Lupfer, C.; Kanneganti, T.D.; et al. The ketone metabolite β-hydroxybutyrate blocks NLRP3 inflammasome–mediated inflammatory disease. *Nat. Med.* **2015**, *21*, 263–269. [CrossRef] [PubMed]
109. Pujol-Lereis, L.M.; Schäfer, N.; Kuhn, L.B.; Rohrer, B.; Pauly, D. Interrelation Between Oxidative Stress and Complement Activation in Models of Age-Related Macular Degeneration. *Retin. Degener. Dis. Mech. Exp. Ther.* **2016**, *854*, 87–93.
110. Ding, J.D.; Kelly, U.; Groelle, M.; Christenbury, J.G.; Zhang, W.; Bowes Rickman, C. The role of complement dysregulation in AMD mouse models. *Adv. Exp. Med. Biol.* **2014**, *801*, 213–219. [CrossRef]
111. Toomey, C.B.; Johnson, L.V.; Bowes Rickman, C. Complement factor H in AMD: Bridging genetic associations and pathobiology. *Prog. Retin. Eye Res.* **2018**, *62*, 38–57. [CrossRef]
112. Hadziahmetovic, M.; Kumar, U.; Song, Y.; Grieco, S.; Song, D.; Li, Y.; Tobias, J.W.; Dunaief, J.L. Microarray analysis of murine retinal light damage reveals changes in iron regulatory, complement, and antioxidant genes in the neurosensory retina and isolated RPE. *Investig. Opthalmol. Vis. Sci.* **2012**, *53*, 5231–5241. [CrossRef] [PubMed]
113. Rutar, M.; Natoli, R.; Albarracin, R.; Valter, K.; Provis, J. 670-nm light treatment reduces complement propagation following retinal degeneration. *J. Neuroinflamm.* **2012**, *9*, 257. [CrossRef] [PubMed]
114. Zhang, M.; Jiang, N.; Chu, Y.; Postnikova, O.; Varghese, R.; Horvath, A.; Cheema, A.K.; Golestaneh, N. Dysregulated metabolic pathways in age-related macular degeneration. *Sci. Rep.* **2020**, *10*, 2464. [CrossRef] [PubMed]
115. Liu, A.; Lin, Y.; Terry, R.; Nelson, K.; Bernstein, P.S. Role of long-chain and very-long-chain polyunsaturated fatty acids in macular degenerations and dystrophies. *Clin. Lipidol.* **2011**, *6*, 593–613. [CrossRef]
116. Sato, N.; Morishita, R. The roles of lipid and glucose metabolism in modulation of β-amyloid, tau, and neurodegeneration in the pathogenesis of Alzheimer disease. *Front. Aging Neurosci.* **2015**, *7*, 199. [CrossRef]
117. Samuel, V.T.; Petersen, K.F.; Shulman, G.I. Lipid-induced insulin resistance: Unravelling the mechanism. *Lancet* **2010**, *375*, 2267–2277. [CrossRef]
118. Chung, K.W. Advances in Understanding of the Role of Lipid Metabolism in Aging. *Cells* **2021**, *10*, 880. [CrossRef]
119. Curcio, C.A.; Presley, J.B.; Malek, G.; Medeiros, N.E.; Avery, D.V.; Kruth, H.S. Esterified and unesterified cholesterol in drusen and basal deposits of eyes with age-related maculopathy. *Exp. Eye Res.* **2005**, *81*, 731–741. [CrossRef]
120. Neale, B.M.; Fagerness, J.; Reynolds, R.; Sobrin, L.; Parker, M.; Raychaudhuri, S.; Tan, P.L.; Oh, E.C.; Merriam, J.E.; Souied, E.; et al. Genome-wide association study of advanced age-related macular degeneration identifies a role of the hepatic lipase gene (LIPC). *Proc. Natl. Acad. Sci. USA* **2010**, *107*, 7395–7400. [CrossRef]
121. Vavvas, D.G.; Daniels, A.B.; Kapsala, Z.G.; Goldfarb, J.W.; Ganotakis, E.; Loewenstein, J.I.; Young, L.H.; Gragoudas, E.S.; Eliott, D.; Kim, I.K.; et al. Regression of Some High-risk Features of Age-related Macular Degeneration (AMD) in Patients Receiving Intensive Statin Treatment. *EBioMedicine* **2016**, *5*, 198–203. [CrossRef] [PubMed]
122. Chen, W.; Stambolian, D.; Edwards, A.O.; Branham, K.E.; Othman, M.; Jakobsdottir, J.; Tosakulwong, N.; Pericak-Vance, M.A.; Campochiaro, P.A.; Klein, M.L.; et al. Genetic variants near TIMP3 and high-density lipoprotein-associated loci influence susceptibility to age-related macular degeneration. *Proc. Natl. Acad. Sci. USA* **2010**, *107*, 7401–7406. [CrossRef]
123. Golestaneh, N.; Chu, Y.; Xiao, Y.-Y.; Stoleru, G.L.; Theos, A.C. Dysfunctional autophagy in RPE, a contributing factor in age-related macular degeneration. *Cell Death Dis.* **2018**, *8*, e2537. [CrossRef]
124. Paterno, J.J.; Koskela, A.; Hyttinen, J.M.T.; Vattulainen, E.; Synowiec, E.; Tuuminen, R.; Watala, C.; Blasiak, J.; Kaarniranta, K. Autophagy Genes for Wet Age-Related Macular Degeneration in a Finnish Case-Control Study. *Genes* **2020**, *11*, 1318. [CrossRef]
125. Orozco, L.D.; Chen, H.H.; Cox, C.; Katschke, K.J., Jr.; Arceo, R.; Espiritu, C.; Caplazi, P.; Nghiem, S.S.; Chen, Y.J.; Modrusan, Z.; et al. Integration of eQTL and a Single-Cell Atlas in the Human Eye Identifies Causal Genes for Age-Related Macular Degeneration. *Cell Rep.* **2020**, *30*, 1246–1259.e1246. [CrossRef] [PubMed]
126. Pan, Y.; Fu, Y.; Baird, P.N.; Guymer, R.H.; Das, T.; Iwata, T. Exploring the contribution of ARMS2 and HTRA1 genetic risk factors in age-related macular degeneration. *Prog. Retin. Eye Res.* **2022**, 101159. [CrossRef]

127. Klipfel, L.; Cordonnier, M.; Thiébault, L.; Clérin, E.; Blond, F.; Millet-Puel, G.; Mohand-Saïd, S.; Goureau, O.; Sahel, J.-A.; Nandrot, E.F.; et al. A Splice Variant in SLC16A8 Gene Leads to Lactate Transport Deficit in Human iPS Cell-Derived Retinal Pigment Epithelial Cells. *Cells* **2021**, *10*, 179. [CrossRef]
128. Melo, E.; Oertle, P.; Trepp, C.; Meistermann, H.; Burgoyne, T.; Sborgi, L.; Cabrera, A.C.; Chen, C.Y.; Hoflack, J.C.; Kam-Thong, T.; et al. HtrA1 Mediated Intracellular Effects on Tubulin Using a Polarized RPE Disease Model. *EBioMedicine* **2018**, *27*, 258–274. [CrossRef] [PubMed]
129. den Hollander, A.I.; Mullins, R.F.; Orozco, L.D.; Voigt, A.P.; Chen, H.-H.; Strunz, T.; Grassmann, F.; Haines, J.L.; Kuiper, J.J.W.; Tumminia, S.J.; et al. Systems genomics in age-related macular degeneration. *Exp. Eye Res.* **2022**, *225*, 109248. [CrossRef]
130. Yamamoto, H.; Yakushijin, K.; Kusuhara, S.; Escaño, M.F.; Nagai, A.; Negi, A. A novel RDH5 gene mutation in a patient with fundus albipunctatus presenting with macular atrophy and fading white dots. *Am. J. Ophthalmol.* **2003**, *136*, 572–574. [CrossRef]
131. Kutty, R.K.; Samuel, W.; Boyce, K.; Cherukuri, A.; Duncan, T.; Jaworski, C.; Nagineni, C.N.; Redmond, T.M. Proinflammatory cytokines decrease the expression of genes critical for RPE function. *Mol. Vis.* **2016**, *22*, 1156.
132. Behrendt, M. TRPM3 in the eye and in the nervous system—From new findings to novel mechanisms. *Biol. Chem.* **2022**, *403*, 859–868. [CrossRef] [PubMed]
133. Held, K.; Tóth, B.I. TRPM3 in Brain (Patho)Physiology. *Front. Cell Dev. Biol.* **2021**, *9*, 635659. [CrossRef]
134. Shiels, A. TRPM3_miR-204: A complex locus for eye development and disease. *Hum. Genom.* **2020**, *14*, 7. [CrossRef]
135. Zhang, C.; Miyagishima, K.J.; Dong, L.; Rising, A.; Nimmagadda, M.; Liang, G.; Sharma, R.; Dejene, R.; Wang, Y.; Abu-Asab, M.; et al. Regulation of phagolysosomal activity by miR-204 critically influences structure and function of retinal pigment epithelium/retina. *Hum. Mol. Genet.* **2019**, *28*, 3355–3368. [CrossRef]
136. Adijanto, J.; Castorino, J.J.; Wang, Z.X.; Maminishkis, A.; Grunwald, G.B.; Philp, N.J. Microphthalmia-associated transcription factor (MITF) promotes differentiation of human retinal pigment epithelium (RPE) by regulating microRNAs-204/211 expression. *J. Biol. Chem.* **2012**, *287*, 20491–20503. [CrossRef] [PubMed]
137. Naylor, J.; Li, J.; Milligan, C.J.; Zeng, F.; Sukumar, P.; Hou, B.; Sedo, A.; Yuldasheva, N.; Majeed, Y.; Beri, D.; et al. Pregnenolone sulphate- and cholesterol-regulated TRPM3 channels coupled to vascular smooth muscle secretion and contraction. *Circ. Res.* **2010**, *106*, 1507–1515. [CrossRef] [PubMed]
138. Bamps, D.; Vriens, J.; Hoon, J.d.; Voets, T. TRP Channel Cooperation for Nociception: Therapeutic Opportunities. *Annu. Rev. Pharmacol. Toxicol.* **2021**, *61*, 655–677. [CrossRef]
139. Su, S.; Yudin, Y.; Kim, N.; Tao, Y.-X.; Rohacs, T. TRPM3 Channels Play Roles in Heat Hypersensitivity and Spontaneous Pain after Nerve Injury. *J. Neurosci.* **2021**, *41*, 2457–2474. [CrossRef]
140. Philp, N.J.; Yoon, H.; Grollman, E.F. Monocarboxylate transporter MCT1 is located in the apical membrane and MCT3 in the basal membrane of rat RPE. *Am. J. Physiol.* **1998**, *274*, R1824–R1828. [CrossRef]
141. Fernandez-Godino, R.; Garland, D.L.; Pierce, E.A. Isolation, culture and characterization of primary mouse RPE cells. *Nat. Protoc.* **2016**, *11*, 1206–1218. [CrossRef]
142. Patro, R.; Duggal, G.; Love, M.I.; Irizarry, R.A.; Kingsford, C. Salmon provides fast and bias-aware quantification of transcript expression. *Nat. Methods* **2017**, *14*, 417–419. [CrossRef]
143. Frankish, A.; Diekhans, M.; Jungreis, I.; Lagarde, J.; Loveland, J.E.; Mudge, J.M.; Sisu, C.; Wright, J.C.; Armstrong, J.; Barnes, I.; et al. GENCODE 2021. *Nucleic Acids Res.* **2021**, *49*, D916–D923. [CrossRef]
144. Love, M.I.; Huber, W.; Anders, S. Moderated estimation of fold change and dispersion for RNA-seq data with DESeq2. *Genome Biol.* **2014**, *15*, 550. [CrossRef]
145. Durinck, S.; Spellman, P.T.; Birney, E.; Huber, W. Mapping identifiers for the integration of genomic datasets with the R/Bioconductor package biomaRt. *Nat. Protoc.* **2009**, *4*, 1184–1191. [CrossRef]
146. Tripathi, S.; Pohl, M.O.; Zhou, Y.; Rodriguez-Frandsen, A.; Wang, G.; Stein, D.A.; Moulton, H.M.; DeJesus, P.; Che, J.; Mulder, L.C.; et al. Meta- and Orthogonal Integration of Influenza "OMICs" Data Defines a Role for UBR4 in Virus Budding. *Cell Host Microbe* **2015**, *18*, 723–735. [CrossRef]
147. Mootha, V.K.; Lindgren, C.M.; Eriksson, K.-F.; Subramanian, A.; Sihag, S.; Lehar, J.; Puigserver, P.; Carlsson, E.; Ridderstråle, M.; Laurila, E.; et al. PGC-1α-responsive genes involved in oxidative phosphorylation are coordinately downregulated in human diabetes. *Nat. Genet.* **2003**, *34*, 267–273. [CrossRef] [PubMed]
148. Subramanian, A.; Tamayo, P.; Mootha, V.K.; Mukherjee, S.; Ebert, B.L.; Gillette, M.A.; Paulovich, A.; Pomeroy, S.L.; Golub, T.R.; Lander, E.S.; et al. Gene set enrichment analysis: A knowledge-based approach for interpreting genome-wide expression profiles. *Proc. Natl. Acad. Sci. USA* **2005**, *102*, 15545–15550. [CrossRef] [PubMed]
149. Metsalu, T.; Vilo, J. ClustVis: A web tool for visualizing clustering of multivariate data using Principal Component Analysis and heatmap. *Nucleic Acids Res.* **2015**, *43*, W566–W570. [CrossRef] [PubMed]
150. Goedhart, J.; Luijsterburg, M.S. VolcaNoseR is a web app for creating, exploring, labeling and sharing volcano plots. *Sci. Rep.* **2020**, *10*, 20560. [CrossRef]
151. Silvestri, A.; Fiorilli, V.; Miozzi, L.; Accotto, G.P.; Turina, M.; Lanfranco, L. In silico analysis of fungal small RNA accumulation reveals putative plant mRNA targets in the symbiosis between an arbuscular mycorrhizal fungus and its host plant. *BMC Genom.* **2019**, *20*, 1–18. [CrossRef] [PubMed]

152. Szklarczyk, D.; Gable, A.L.; Lyon, D.; Junge, A.; Wyder, S.; Huerta-Cepas, J.; Simonovic, M.; Doncheva, N.T.; Morris, J.H.; Bork, P.; et al. STRING v11: Protein-protein association networks with increased coverage, supporting functional discovery in genome-wide experimental datasets. *Nucleic Acids Res.* **2019**, *47*, D607–D613. [CrossRef] [PubMed]
153. Szklarczyk, D.; Gable, A.L.; Nastou, K.C.; Lyon, D.; Kirsch, R.; Pyysalo, S.; Doncheva, N.T.; Legeay, M.; Fang, T.; Bork, P.; et al. The STRING database in 2021: Customizable protein-protein networks, and functional characterization of user-uploaded gene/measurement sets. *Nucleic Acids Res.* **2021**, *49*, D605–D612. [CrossRef] [PubMed]